Designing an Induction Wind Tunnel

Internship Assignment
National Research Council Canada

Dimar Detert Oude Weme
Master Student Mechanical Engineering,
Chair Engineering Fluid Dynamics

Internship report

This report is about my internship performed at the National Research Council Canada (NRC) in Ottawa. The internship is part of the curriculum of the master Mechanical Engineering at the University of Twente.

Carried out by:	D.G.J. Detert Oude Weme
	S0197009
Host institution:	National Research Council Canada
	Ottawa, Canada
Supervisor host institution:	Dr. Jerry Syms
Home institution:	University of Twente
	Enschede, The Netherlands
Supervisor home institution:	Prof. Dr. Ir. H.W.M. Hoeijmakers
Duration of the internship:	July 8th 2014 - October 17th 2014

Summary

A one-dimensional analysis has been performed on an induction wind tunnel, with a constant mixing section. Compressed air is injected into the back end of the tunnel by a simple converging-diverging nozzle; this induces a flow through the tunnel. The analysis is based on the conservation equations of mass, momentum and energy, where it is assumed the flow is isentropic throughout the tunnel and nozzle. The areas used in this report for the calculations are based on optimal area ratios investigated by Watanawanavet [6], and minimum required that are needed to fit test objects (fuselage panels). Some pointers and tips for setting up the Computational Fluid Dynamics (CFD) simulations are then given. Finally other ejector systems are recommended, which may have a positive influence on the performance of an induction tunnel. These can be used to test and optimize the injection system of the tunnel with CFD.

Preface

This internship was performed at the National Research Council Canada (NRC) in Ottawa, as part of the curriculum of the Master Mechanical Engineering at the University of the Twente. The internship is 15 to 20 European Credits (EC), depending on the length of the internship. It is an opportunity for the Master student to apply his knowledge in a company and gain some working experience. This can be done abroad to experience another country and culture or in the Netherlands.

This report covers the project that I worked on during my internship in the period July 8 - October 17. My internship originally consisted of designing the injector/ejector system of a turbulent boundary layer transmission loss facility with 2D and eventually 3D Computational Fluid Dynamics (CFD) simulations, under the Working and Traveling on Aircraft (WTA) program at the NRC. This facility would be able to determine how much sound of the air flowing over the fuselage skin is transmitted into the aircraft cabin. This unique wind tunnel would be driven by a compressed air storage system that already has been built at the NRC. The efficiency of this wind tunnel is greatly determined by how the air gets introduced into the circuit of the turbulent boundary layer wind tunnel.

Unfortunately during my time working at the NRC for my internship, there was a cyber intrusion. For me this was bad luck, because all the servers and computers that were used to run the grid generator and CFD programs like Gridgen/Pointwise and Cobalt could not be used anymore. Because of this I lost a fair amount of data, designs and time and could not perform any CFD simulations. This is why this report is lacking the desired 2D and 3D CFD simulations, designs and solutions for the induction tunnel and ejector system and instead there is focused on an one-dimensional analysis of an induction wind tunnel. There is a CFD chapter, which contains some pointers and other things I encountered and learned in the short time that I was still able to use the CFD software.

During my internship at the NRC I worked with Dr. Jerry Syms, who was my supervisor during my internship. I am grateful to him for giving me the opportunity to work at the NRC. And I want to thank him for guiding me during the project and for making me feel welcome at the NRC. I would also like to thank Professor Hoeijmakers, who was my supervisor at the University of Twente at the Engineering Fluid Dynamics during this project, for giving me the opportunity to go to the NRC in Canada.

Contents

1 Introduction

Traveling by plane has become one of the most popular ways to travel and the air transport industry still keeps growing continuously. Developing countries are growing the fastest with up to 12 percent a year. Although the growth in Europe and North America is not as big anymore, it is still growing every year. According to the International Air Transport Association (IATA) the average growth rate for the air travel markets around the world are still about 5 percent every year [1]. Airlines expect to see a 31 percent increase in passenger numbers between 2012 and 2017. The total passenger numbers are then expected to be 3.91 billion, this is an increase of 930 million passengers compared to 2012 [2].

This means passenger comfort will get more and more important. One of the factors that increases passenger comfort is noise reduction. The three most important aeroacoustic noise sources in aircraft cabins are the turbulent boundary layer (TBL) on the fuselage, the jet noise and the air conditioning system (ACS). The TBL-induced noise is the most dominant contributor during cruise at lower flight speeds and higher flight speeds at all flight levels. The TBL-induced cabin noise increases by 3 to 4 dB(A) when moving back and forth through the cabin and it rises with decreasing flight level and increasing flight speed [3]. By understanding the pressure fluctuations in the TBL and reducing the amount of noise transmitted through excitation of the fuselage panels into the cabin, there is potential to greatly enhance passenger comfort.

The pressure fluctuations within a TBL have been studied in detail, but most of the research that has been done is focused on low Mach number flows or very high (supersonic) Mach number flows. Many empirical models like Chase, Corcos and Efimstov have been developed from this research to describe the turbulent boundary layer wall pressure fluctuations on a flat plate. These models are used in computational simulations to predict the transmission loss through a structure for the turbulent boundary layer noise. Recently, more studies have started looking at high subsonic Mach number flows, like the Mach numbers that aircrafts would encounter and they indicate that more research is needed to measure the accuracy of the models as well as their applicability to curved surfaces such as a fuselage [4].

2 Turbulent boundary layer and transmission loss wind tunnel

At the NRC, the Aerodynamics Laboratory does a lot of research in the field of aeroacoustics, especially research in reducing the noise associated with airplanes. This is all part of the Working and Traveling on Aircraft (WTA) program. Within this program, new technology solutions are provided to airline companies to improve the passenger comfort and reduce the costs of flying. But currently there is no combined turbulent boundary layer and transmission loss wind tunnel that can operate at high subsonic speeds which can match the Mach number seen during flights (in this case a cruise speed of Mach 0.85 that represents the speed of a typical business jet). Such a wind tunnel would be able to measure the pressure fluctuations and transmission losses through an actual curved fuselage panel excited by a realistic turbulent boundary layer at high subsonic speeds. This facility would be unique and could potentially be used to refine computational models and help with developing noise reduction technologies for fuselage panels and thus potentially improve the comfort of airplane passengers.

2.1 Induction wind tunnel

Wind tunnels can be used to simulate the flow conditions of airplanes during flight. They generally consist of a source that provides the flow like a fan or a compressor, a nozzle that accelerates the flow, the test section and a diffuser to decelerate the flow and to recover the pressure.

Wind tunnels can be divided into two different groups, namely the open and closed return wind tunnel. The open return wind tunnel is also called an Eiffel tunnel named after the French engineer Gustave Eiffel. This type of tunnel is open at both the end and the beginning and uses the atmospheric air of the room where the wind tunnel is in. This tunnel is usually driven by a fan, blower or compressor either before or after the test section of the tunnel. When the fan or compressor is located after the test section it is entrains the air into the tunnel.

These tunnels are low in construction costs, but are often very noisy and have a lot of vibrations because of the fan.They require some sort flow straighteners to eliminate flow disruption from the inlet.

The closed return wind tunnel, also called a Prandtl tunnel after the German engineer, a or Gottingen tunnel after the German research laboratory, is a tunnel that is a loop where the outlet is connected to the inlet. So the air is only circulating in the tunnel, instead of drawing or blowing atmospheric air into the tunnel. These tunnels are usually used for longer test durations. These tunnels have better flow quality and have less operating costs as they do not constantly need to accelerate the air, but they have higher construction cost as they are bigger and require guide vanes and a different infrastructure.

The boundary layer wind tunnel that has been conceived has to generate a flow that has minimal to no influence from external factors such as noise, vibration and aerodynamic disturbances. An efficient, cheap and relatively silent way to do this is with an open induction type wind tunnel, driven by a compressor. An induction tunnel is cheaper to build and maintain than a blow down tunnel, because there are no actual moving parts (fans) in the tunnel. The NRC also has a large compressor with large storage tanks available already, which also helps to cut down costs and keep noise and vibrations to a minimum. An induction wind tunnel injects compressed air into the back end of the wind tunnel (after the test section, but well before the diffuser), which will be called the primary flow in this report. This air then entrains atmospheric air, called the secondary flow, from the beginning of the tunnel through the test section. This is due to the pressure difference and shear layers created by the mixing of the two flows. The two flows start to mix and exchange energy after the ejector in the section called the mixing chamber. During this mixing the flows will slow down and recovery some pressure. The way the primary flow is injected into the tunnel has a great impact on the efficiency of the tunnel.

2.1.1 Concept tunnel

A concept induction tunnel has already been developed by Dr. J. Syms. The components of the concept tunnel can be found in figure 2.1, some key components of the tunnel that have a large influence on its performance are discussed briefly below.

Inlet

The inlet of the boundary tunnel needs to ensure a smooth uniform and silent flow. This is done by introducing a bell mouth, silencer and a turbulent screen. After that there needs to be a converging section to accelerate the flow. This section needs to converge in such a way so there is no flow separation that will disturb the flow.

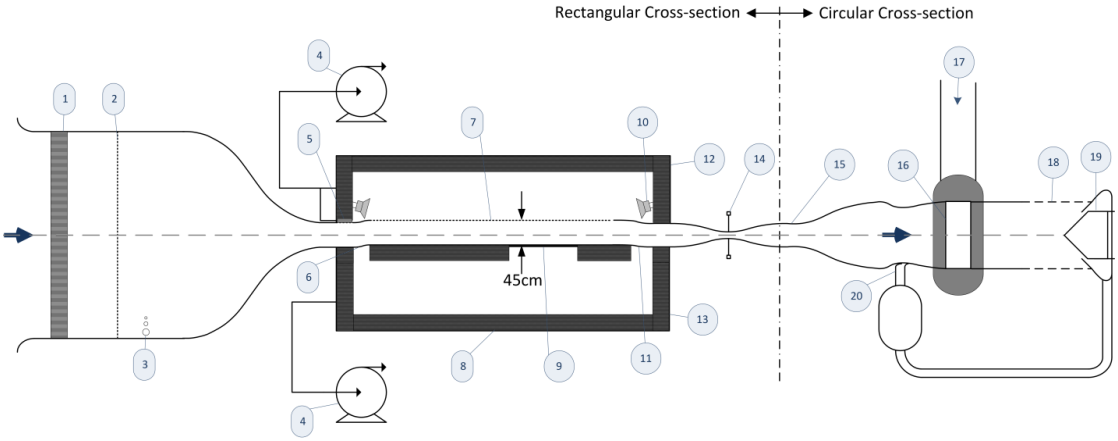

1. Silencer
2. Turbulence Screen
3. Boundary Layer Profiler
4. Vacuum Pumps
5. Boundary Layer Suction
6. Profiled Leading Edge
7. Porous Kevlar Screen
8. Acoustic Treatment
9. Test Article (1.25m x 0.5m)
10. Speakers
11. Profiled Trailing Edge
12. Sealed Plenum Chamber (Test Section Pressure)
13. Sealed Plenum Chamber (Fuselage Cabin Pressure)
14. Sonic Throat with Profiling Actuators
15. Cross-section Transition
16. Supersonic Petal Nozzle Ejector
17. 300PSI Compressed Air
18. Porous Mesh Bucket
19. Adjustable Tail Cone with Vaned Volute
20. Coanda Effect Ejector

Figure 2.1: Transmission loss and turbulent boundary layer tunnel concept

Test section

The test section is where the test article, in this case a fuselage panel, is located. This section is directly after the converging section mentioned above. The conditions here need to be the same as the flight conditions. This is why there are sealed plenum chambers to create the right pressures that mimic the pressures of the atmospheric conditions outside and inside the plane.

To grow a sufficiently large boundary layer in the test section, that represents a turbulent boundary layer on a fuselage of an airplane during flight, the tunnel needs to have a long working section. This way the object (the fuselage panel in this case) can also be placed in different sections of the test section so it can be tested with different boundary layers heights. The TBL on an airplane during flight can be as large as 25 cm on an actual airplane [7], so also the height of the tunnel needs to be taken in consideration. The area ratios of the test section greatly determine the pressures and thus energy needed to create the right velocity in the test section.

Since there is no upper wall when an airplane is airborne and in order to let the turbulent boundary layer on the fuselage panel grow to the right size with no interference of the upper wall, a porous wall and vacuum pumps have been included, that suck away the boundary layer growing on the upper wall of the wind tunnel.

Ejector system

The ejector or injector system is an important part of the induction wind tunnel as it propels the primary stream into the tunnel, which then entrains the secondary flow. The type and geometry of the ejector system greatly determines the efficiency of the wind tunnel. Various ejectors systems can be used which will be discussed later. In general shocks should be kept to a minimum because they introduce pressure losses and turbulence into the system, which dissipate energy. This means that the injector should be designed to transfer as much energy from the primary flow to the secondary flow as possible. This can be obtained by investigating various geometries and the position of the ejector as well as different systems.

Mixing section

The section where the primary and secondary stream join is called the mixing section. The interaction between these two streams is very important and has a large influence on the efficiency of the tunnel. If more shear layers exist, the two flows will mix better; this draws in even more of the secondary flow which makes the wind tunnel more efficient. There are two conventional ways to mix the fluids. With a constant pressure and with a constant area section. The constant area mixing section is believed to have better mixing than the constant pressure mixing section. The interaction between the shocks from the supersonic nozzle and the wall boundary layer in a constant pressure mixing section is noticeably stronger than in a constant area jet ejector. This means that there will be a stronger turbulence field and stronger turbulent mixing decreases the ejector's performance [6].

The mixing should be finished before the mixing section ends in order to take advantage of the maximum pressure recovery in the diffuser [9]. The optimum mixing section length should be between 5 and 10 times the mixing section diameter to operate within three percent of the optimum performance [6].

Because the primary stream is normally supersonic and because it is slowed down by the induced secondary stream relatively sudden, large velocity and pressure gradients between the two streams may be present, which can lead to shock waves. Reflections of these shock waves could lead to a multiple shock system [9].

Pressure recovery

Normally a wind tunnel has some sort of subsonic diffuser. The diffuser slows the flow down due to the increasing cross sectional area, which recovers some of the pressure energy. This energy can be recycled into the wind tunnel's circuit. The expansion rate of the diffuser is an important parameter. If the diffuser angle is too large, it can cause flow separation, which dissipates energy. The concept tunnel makes use of an adjustable

tail cone to recover the pressure and a porous mesh bucket to control how much energy is recycled and exhausted [4].

Sonic throat

To measure the sound created by the TBL on the fuselage, while trying to keep the disturbances by the environment and tunnel to a minimum, there is placed a sonic throat in the conceptual tunnel after the working section and before the ejector system. The Mach number just reaches unity at the throat. This way the sound that is generated after the test section cannot travel upstream and interfere with the measurements in the test section.

The throat has to be designed in such a way that the sound cannot travel upstream (Mach 1 at the throat). But shocks need to be minimized to prevent pressure losses. This means that the throat should be designed so that it is shock free and expands isentropically.

3 1D-analysis for an ideal induction wind tunnel

To determine some of the general aerodynamic properties like pressure, cross sectional area and entrainment ratio of the conceptual tunnel, a one-dimensional analysis for an ideal induction wind tunnel is performed on the simplified basic wind tunnel as drawn below, which can be used to confirm future CFD solutions:

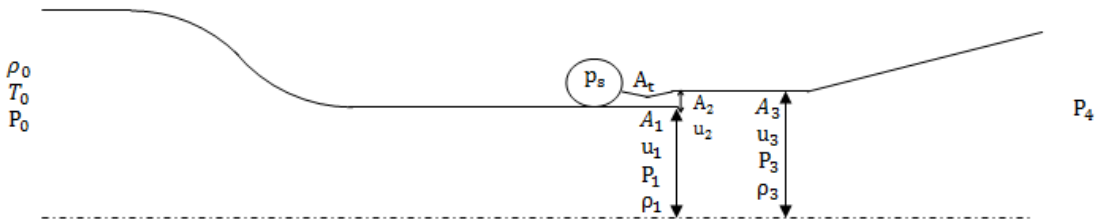

Figure 3.1: Simple one dimensional tunnel description

The design that is used for this one-dimensional analysis is a simple wind tunnel with a converging and diverging section, but with an ejector and a constant area mixing section. This ejector is, in this case, a simple convergent-divergent nozzle. Because the wind tunnel is symmetric, only the top half of the tunnel is used. This is the tunnel to get the first parameters and solutions from to set up a first design and confirm CFD solutions.
The following equations and solutions apply for a constant area mixing section, as it is believed this has less losses than the constant pressure mixing section, as stated before.

The exiting velocity from the ejector is supersonic. It is assumed that the ejector expands and contracts isentropically in such a way that the ejector is ideal and the primary and secondary streams have equal static pressures ($p_1 = p_2$) at the exit of the ejector. This means that no shock waves are present. It is further assumed that wall shear forces are negligible compared to the pressure and momentum forces of the primary and secondary streams. There is no heat transferred across the walls and thus the system is considered to be adiabatic.

The flows are assumed to be compressible, steady, reversible and inviscid, and the fluid

is assumed to be a calorically perfect gas with $p = \rho RT$, $h = c_p T$ and $R = c_p - c_v = 287 Jkg^{-1}K^{-1}$, with no external body forces. This means that turbulence, shear layers and shocks are not accounted for. All are present in the real case of an induction tunnel and will most certainly have an effect on the performance and efficiency of the wind tunnel.

Since the mixing section area is assumed constant, the areas can be related through the following equations.

$$A_3 = A_2 + A_1 \tag{3.1}$$

$$\frac{A_2}{A_3} << 1 \tag{3.2}$$

The following conservation equations [5] apply to the tunnel:

Conservation of Mass:

$$A_3 u_3 \rho_3 = A_2 u_2 \rho_2 + A_1 u_1 \rho_1 \tag{3.3}$$

$$\dot{m}_3 = \dot{m}_2 + \dot{m}_1 \tag{3.4}$$

Conservation of Momentum:

$$A_3(p_1 - p_3) = A_3 u_3^2 \rho_3 - (A_2 u_2^2 \rho_2 + A_1 u_1^2 \rho_1) \tag{3.5}$$

Conservation of Energy:

$$\left(\frac{\gamma}{(\gamma-1)}\frac{p_3}{\rho_3} + \frac{u_3^2}{2}\right)\rho_3 u_3 A_3 = \left(\frac{\gamma}{(\gamma-1)}\frac{p_1}{\rho_1} + \frac{u_1^2}{2}\right)\rho_1 u_1 A_1 + \left(\frac{\gamma}{(\gamma-1)}\frac{p_2}{\rho_2} + \frac{u_2^2}{2}\right)\rho_2 u_2 A_2 \tag{3.6}$$

With these equations and the tunnel's design and operating conditions in test section and ejector system known or specified, the solutions ρ_3, p_3 and u_3 in the mixing section can be calculated. From these solutions other equations can be derived again, if needed.

The pressure ratio between the test section and the atmospheric conditions outside of the wind tunnel, p_1/p_0, and the pressure ratio between the reservoir and the stream in the test section, p_s/p_1, can be evaluated through isentropic relations

$$\frac{p_1}{p_0} = \left(\frac{1}{1 + \frac{\gamma-1}{2}M_1^2}\right)^{\frac{\gamma}{\gamma-1}} \tag{3.7}$$

$$\frac{p_s}{p_2} = \frac{p_s}{p_1} = \left(1 + \frac{\gamma-1}{2}M_2^2\right)^{\frac{\gamma}{\gamma-1}} \tag{3.8}$$

Note that $p_s/p_2 = p_s/p_1$ is assumed. The Mach number of the test section (M_1) and the Mach number at the exit of the nozzle (M_2) are needed in order to calculate these pressure ratios. This can be seen from equations 3.7 and 3.8. M_1 is known, since this is the operating condition of the wind tunnel, which in this case is $M_1 = 0.85$. M_2 is still unknown, but depends on the pressure of the compressor and the back pressure of the nozzle. The back pressure in this case is assumed to be equal to the pressure in the test section. This pressure can be obtained from the Mach number needed in the test section, M_1.

The compressor that is available at the NRC contains 44000 lbs (or 20000 kg) of air at a pressure of 300 psi (2068 kPa). This means that the compression ratio $\lambda = p_s/p_0$ is set at 20.4, with $p_0 = 101.3kPa$. The compression ratio can be calculated with the following formula:

$$\lambda = \frac{p_s}{p_0} = \frac{1}{\frac{p_0}{p_1}} \frac{p_s}{p_1} = \left(\frac{1 + \frac{\gamma-1}{2} M_2^2}{1 + \frac{\gamma-1}{2} M_1^2} \right)^{\frac{\gamma}{\gamma-1}} \tag{3.9}$$

Equation 3.9 can be rewritten in order to calculate M_2 as a function of the compression ratio λ and M_1 to:

$$M_2^2 = \frac{(2 + (\gamma-1)M_1^2)\lambda^{\frac{\gamma-1}{\gamma}} - 2}{\gamma - 1} \tag{3.10}$$

Now that p_1 can be evaluated and M_1, M_2 and p_0 are known, a solution can be found for p_3 through the pressure ratio p_3/p_1. With a significant manipulation of the (conservation) equations (see Appendix A.1), the ratio $\frac{p_3}{p_1}$ can be found, that now only depends on the variables M_1, M_2 and the area ratio A_2/A_1.

$$\frac{p_3}{p_1} = \frac{1}{(\gamma-1)} \left(1 + \gamma \frac{M_1^2 + \frac{A_2}{A_1} M_2^2}{(1 + \frac{A_2}{A_1})} \right) \tag{3.11}$$
$$+ \gamma \sqrt{\frac{\gamma^2}{(\gamma+1)^2} \left(1 + \gamma \frac{M_1^2 + \frac{A_2}{A_1} M_2^2}{(1 + \frac{A_2}{A_1})} \right)^2 - \left(\frac{M_1^2 \sqrt{\frac{2}{M_1^2} + \gamma - 1}}{(\gamma+1)(1 + \frac{A_2}{A_1})} + \frac{\frac{A_2}{A_1} M_2^2 \sqrt{\frac{2}{M_2^2} + \gamma - 1}}{(\gamma+1)(1 + \frac{A_2}{A_1})} \right)^2}$$

With this equation p_3/p_1 can be evaluated for different ratios of A_2/A_1 for a specified M_1, λ and thus M_2. u_3 and thus M_3 can also be obtained from the energy equation (see appendix A.3).

Since the exit velocity of the ejector depends on the geometry of the ejector, namely the area ratio between the exit and throat, A_2/A_t, it can be calculated. In order to calculate the ratio A_2/A_t, the Mach number area equation is used, where A_t is assumed sonic ($A_t = A^*$) at all times. The equation is based on the well known isentropic flow relations, so a flow without shock waves is considered, as mentioned before. The equation that relates the Mach number to the area is as follows [8]:

$$\frac{A(x)}{A^*} = \sqrt{\frac{1}{M(x)^2}\left[\left(\frac{2}{\gamma+1}\right)\left(1+\frac{\gamma-1}{2M(x)^2}\right)\right]^{\frac{\gamma+1}{\gamma-1}}} \tag{3.12}$$

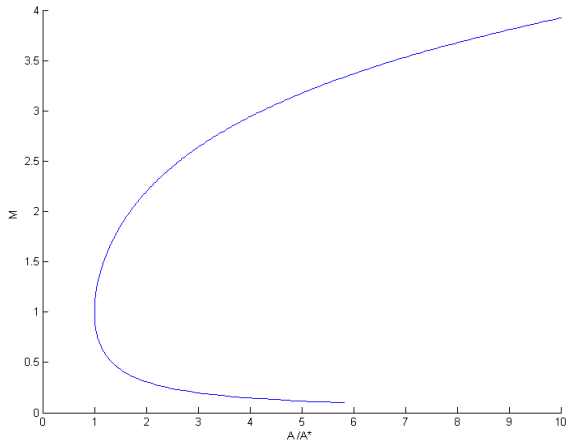

Figure 3.2: Mach number vs A_2/A^*

where x denotes the location within the nozzle. Equation 3.12 is used to plot the Mach number of the nozzle as a function of the area ratio in figure 3.2. For values below zero the flow is subsonic and represents the converging section of the nozzle. For supersonic values, it represents the diverging section and it can be used to determine the cross sectional area at a certain Mach number at the exit. For the diverging section, the Mach number gets bigger rapidly as the cross section area increases. The corresponding back pressure p_2 of the nozzle can be obtained through the isentropic relations mentioned before.

Since M_1 is known and the compression ratio λ is fixed, the desired M_2 can be calculated with equation 3.10. With this M_2 now known, the area ratio of A_2/A_t can be derived with equation 3.12. With A_2/A_t and A_2/A_1 known, the ratio A_t/A_3 can also be

calculated through the following relation:

$$\frac{A_2}{A_1} = \frac{A_2}{A_t}\frac{A_t}{A_3}\frac{A_3}{A_1} \tag{3.13}$$

$$\frac{A_t}{A_3} = \frac{1}{\frac{A_1}{A_2}+1}\frac{1}{\frac{A_2}{A_t}} \tag{3.14}$$

All values can be calculated for different values of M_1, λ and A_2/A_1, as shown in figures 3.3, 3.4 and 3.5. In figure 3.3, the Mach number in the test section is plotted against the Mach number injected by the nozzle. The data point $M_1 = 0.85$ that is the primary operating condition is highlighted.

Figure 3.4 shows the relation between area ratio of the nozzle throat and exit and the test section Mach number. Because A_2/A_t determines M_2, it also determines M_1.

Lastly, figure 3.5 shows the relation between M_1 and the ratio A_t/A_3 for different ratios of A_2/A_1. Here it can be seen that when the throat area of the nozzle is small compared to the mixing section, the test section Mach number is very sensitive to small changes in area.

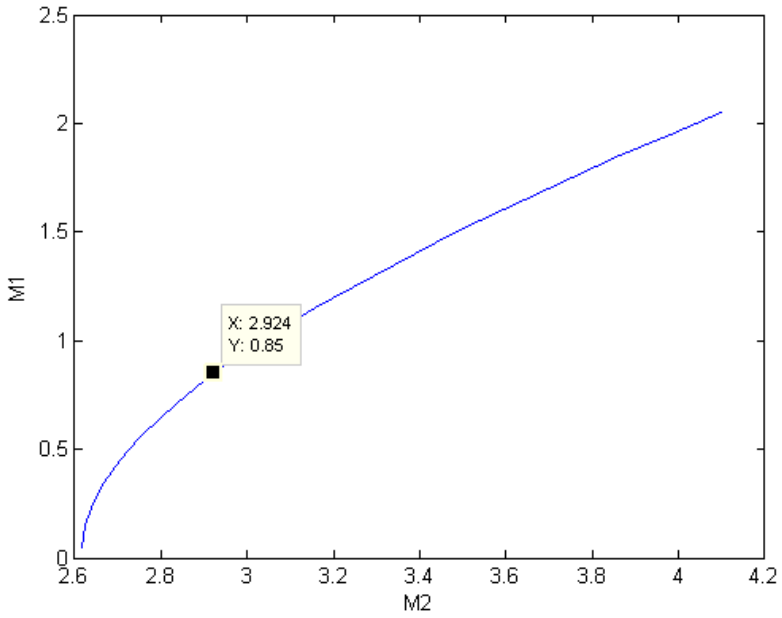

Figure 3.3: Test section Mach number vs Mach number leaving the ejector nozzle

3.1 Calculations

In this section a selection of calculations are performed with the equations mentioned in the previous section. The desired Mach number in the test section is $M_1 = 0.85$, because this is the cruise speed of a typical modern business jet. For this value, it can be seen from figure 3.3 that a Mach number of about $M_2 = 2.9$ is needed to accomplish this with the given compression ratio λ of 20.4 in this configuration.

Area ratios

From figure 3.4, one can see that to achieve an $M_2 = 2.9$ and thus a test section Mach number of $M_1 = 0.85$, a throat ratio of $A_2/A_t = 3.937$ is needed. This figure shows that when the exit area of the nozzle (and the nozzle is expanded isentropically) is larger, the Mach number in the test section will also be higher. Other calculations for a lower velocity in the test section, namely $M_1 = 0.1$, have also been done and are tabulated in table 3.1, in case these are needed to confirm low speed CFD simulations.

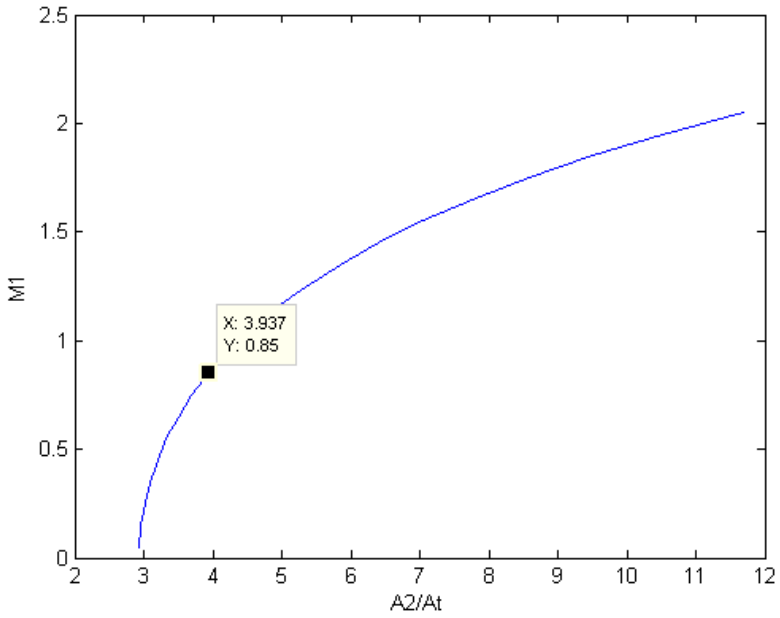

Figure 3.4: Test section Mach number vs A2/At

From figure 3.5 it can be seen how the ratio A_t/A_3 changes for different ratios of A_2/A_1. As the ratio A_2/A_1 gets bigger, A_t/A_3 increases as well with the same settings for M_1 and M_2. In this figure it can also be seen that when A_2/A_1 is larger, the slope of the function becomes less steep. This means that if it is chosen to control the Mach number

in the test section by changing the throat size, it is less sensitive at larger A_2/A_1 ratios.

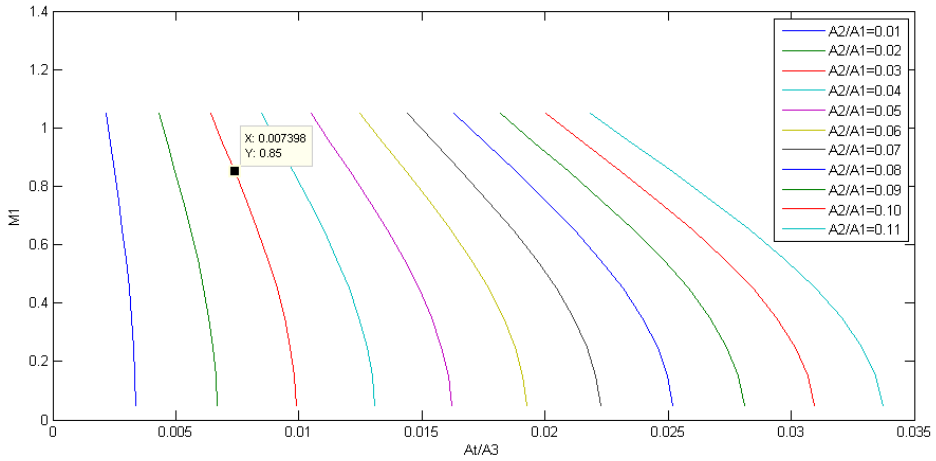

Figure 3.5: Test section Mach number vs At/A3

In order to calculate some values for the areas A_2, A_3 and A_t, the values of A_2/A_1 have to be known beforehand and an A_1 has to be chosen. From Watanawanavet [6] it is known that a good ratio of A_2/A_1 is in the 0.03-0.05 range. Although the definition of A_1 in [6] is a little different (A_2 is included in A_1), the numbers of [6] are used since the area of A_2 is so small compared to A_1. Watanawanavet mentions a ratio of 0.03 for obtaining an M_2 of 3 as the most optimal ratio, this data point is highlighted in figure 3.5 and gives a ratio of A_t/A_3 of 0.007398.

A_1 is set at 22 cm in this case, in order to fit in a whole curved fuselage panel and to let the boundary layer grow sufficiently, this means that the height of the whole tunnel is 44cm. The calculated areas for $M_1 = 0.1$ and $M_1 = 0.85$ are displayed in table 3.1.

M_1	p_s/p_0	M_2	A_2/A_t	$A_1(m)$	A_2/A_1	$A_2(m)$	$A_t(m)$	A_t/A_3	$A_3(m)$
0.85	20.414	2.924	3.937	0.22	0.03	0.0066	0.001676	0.007398	0.2266
					0.04	0.0088	0.002235	0.009769	0.2288
					0.05	0.011	0.002794	0.01209	0.2311
0.1	20.414	2.619	2.949	0.22	0.03	0.0066	0.002238	0.009877	0.2266
					0.04	0.0088	0.002984	0.01304	0.2288
					0.05	0.011	0.00373	0.01615	0.2310

Table 3.1: Wind tunnel area ratios calculated without losses

The data of table 3.1 show that the throat areas are really small and might not be

realistic. With the calculated dimensions, friction and viscosity (think for example of boundary layers) will play a dominant role and may change the flow and its properties significantly. It can also be seen that when A_2 is chosen to be bigger, with a constant A_1, the throat area A_t also needs to be larger to maintain the same M_2. A_3 will of course also be bigger as A_3 is the sum of A_2 and A_1.

Pressure and Mach number

Now that the corresponding areas are either set or calculated, the pressures can also be calculated. p_1 can be found through equation 3.7, which in turn gives p_3 from equation 3.11. p_4 is equal to p_0 as this system is assumed to be ideal with no losses.

From table 3.2, one can see that the pressure in the test section (p_1) has a lower pressure than the flow in the mixing section (p_3). The mixing section has a slightly larger area than the test section and thus also a slightly lower velocity and a higher pressure. This makes sense when thinking of the (incompressible) Bernoulli equation since pressure and velocity are a trade-off. In the mixing section the velocity of the flow is normally also slowed down due to the mixing: the primary flow exchanges its energy to the entrained flow.

M_1	p_s/p_0	$p_0(Pa)$	$p_1(Pa)$	$p_3(Pa)$	$p_4(Pa)$	M_3
0.85	20.4	101235	63178	84890	p_0	0.7243
				90890	p_0	0.7025
				96610	p_0	0.6848
0.1	20.4	101235	100619	124900	p_0	0.1724
				132400	p_0	0.1903
				139700	p_0	0.2062

Table 3.2: Wind tunnel pressures calculated without losses

M_3 is calculated by obtaining u_3 from p_3 as shown in Appendix A.3. It can be seen that the Mach number before entering the diffuser, M_3, is subsonic, which means the subsonic diffuser after the mixing section will slow down the flow even more. While the flow is slowed down inside the expanding area of the diffuser the pressure rises. This is called pressure recovery. A good pressure recovery makes the tunnel more efficient, as there are less losses. The efficiency of the pressure recovery of the diffuser depends on it's angle and configuration, which can be checked through CFD software with various designs.

Again it should be noted that the Mach number M_3 is fairly low compared to the Mach number exiting the nozzle. Since this is an ideal system there are no shocks, but in reality

there will most likely be shocks, to adapt to all the sudden changes of flow properties between the two flows.

Entrainment ratio

The performance of ejectors is often measured through the entrainment ratio. The entrainment ratio is calculated by the mass flow of the secondary stream divided by the mass flow of the primary stream. The mass flow of the primary stream is limited by the throat, as the flow in the nozzle is assumed to be sonic at all times. This means that the mass flow of the primary stream equals the mass flow of the sonic throat. The secondary mass flow rate through the test section (with $2A_1$) and the primary mass flow rate through the sonic throats ($\dot{m}_t$ is the mass flow through $2A_t$) can be evaluated with the mass flow equation and Saint-Venant equation [8], and the properties corresponding to the Mach number in the test section:

$$\dot{m}_1 = 2A_1\rho_1 u_1 \tag{3.15}$$

$$\dot{m}_{t,max} = A^*\sqrt{p_s\rho_s}\sqrt{\frac{2\gamma}{\gamma+1}}\left(\frac{2}{\gamma+1}\right)^{\frac{1}{\gamma-1}} \tag{3.16}$$

M_1	p_s/p_0	$\dot{m_{t,max}}(kg/s)$	$\dot{m}_1(kg/s)$	$\dot{m}_1/\dot{m_{t,max}}$
0.85	20.4	16.236	103.418	6.37
		21.648		4.78
		27.06		3.82
0.1	20.4	10.8372	13.003	1.20
		14.45		0.90
		18.062		0.72

Table 3.3: Wind tunnel entrainment ratios calculated without losses

The Saint-Venant equation used in this case, equation 3.16, is only valid when the throat is choked, as this is the equation for the maximum mass flow (see Appendix A.4). This is also the reason why the maximum mass flow (see table 3.3) goes up when the throat, A_t, is enlarged, as more mass can go through, while the flow remains choked. The density ρ_s is calculated at room temperature ($T_s = 298K$) with the ideal gas law.
The entrainment ratios are not very high, especially for the case with $M_1 = 0.1$; this is due to the high pressure in the tank (p_s) of the compressor, which gives a very high maximum mass flow in the throat.

3.2 Compressor storage tanks

In the previous sections, the supply pressure of the container (p_s) remained constant. To accomplish this however, the compressors would need to run continuously. This means that the cost of a run would be very high. Consequently in this section the alternative that the compressor only fills up the storage tank will be looked at. The pressure in the tanks of the compressor however, will now go down with time was compressed air is exhausted through the supersonic nozzle into the tunnel, this means that the compression ratio $\lambda = p_s/p_0$ will go down over time, which in turn means that M_2, that is a function of λ (see equation 3.10), will start to drop. The consequence of this is that M_1 in the test section will also start to drop, which is undesired. In order to keep the right Mach number in the test section, with A_t of the ejector and thus the mass flow through the throat taken constant, the exit area A_2 of the nozzle has to decrease in such a way that the Mach number in the test section remains constant (see equation 3.12). Note that A_t could also be changed, but for a descriptive manner to see how the flow behaves, it is chosen to (isentropically) change A_2 instead of A_t.
The storage tank has a volume of $V = 1557.43m^3$ and is assumed to have an initial temperature of $T_i = 298K$ with the initial pressure $p_i = 2068427.19Pa$ [4].

The pressure in the storage tank runs down isentropically according to the following equation:

$$p_s(t) = \left(\frac{t \cdot (1-\gamma) R \sqrt{T_i} A_t \sqrt{\frac{\gamma}{R} \left(\frac{2}{\gamma+1}\right)^{\frac{\gamma+1}{\gamma-1}}}}{-2V} + 1 \right)^{\frac{2\gamma}{1-\gamma}} \cdot p_i \tag{3.17}$$

This equation is only valid whenever there is a sonic throat within the nozzle (see appendix A.4). Since the throat area A_t is now fixed and A_2 will be controlled in such a way that the back pressure p_2 and thus M_1 will remain constant. This is only valid in our case for $A_2 \geq A_t$ because at this point the throat will shift to another location (at this point it is not a converging-diverging nozzle, but just a converging nozzle) and M_2 will be subsonic. At this point the back pressure is not low enough. This means that the flow will not become sonic anywhere in the nozzle again and thus also not sonic at the throat anymore. This can be seen in figures 3.8b and 3.8c

First the pressure loss in time is plotted (see figure 3.6) with equation A.66, this graph gives the pressure drop at the three different throat areas for a constant test section Mach number of 0.85. The runtime of the tunnel goes down when a bigger throat is used, this is due to the fact that more mass flow is able to go through, which results in the tank losing air and pressure faster.

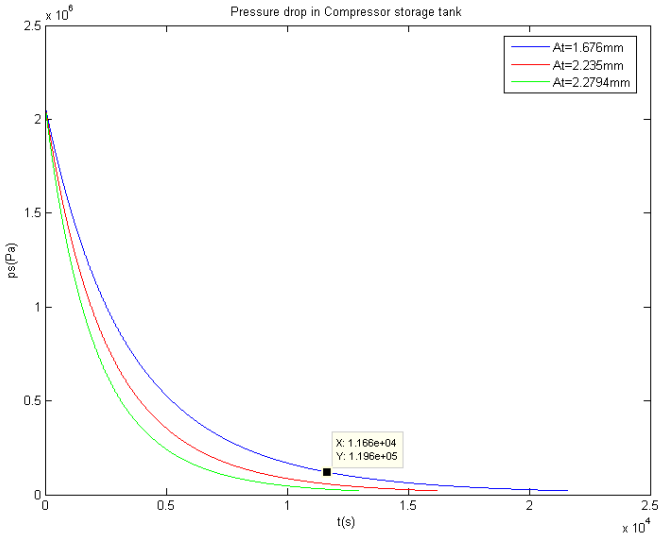

Figure 3.6: Pressure time history in the storage tank, with M_1=0.85

The change of A_2/A_t as a function of t, which is calculated with equation 3.12, which is a function of the Mach number M_2. M_2 is obtained from the change in compression ratio λ, which is a function of time now. To keep M_1 at 0.85, A_2 changes gradually and slowly, as can be seen in figure 3.7, to keep the correct back pressure. If it is chosen to control A_2/A_t it has to be done accurately. Shock waves will exists if this is not done properly, which will cause huge loses in the system and M_2 will be much lower than expected.

From figure 3.2, it can be seen that when M_2 is equal to 1 the area ratio A_2/A_t is also equal to 1, which means the throat area has become the exit area. In this case the equations that are used, are not applicable anymore. Since the throat is no longer choked, the pressure and Mach number needed to get the right Mach number of $M_1 = 0.85$ in the test section are not possible. This means that when A_2/A_t reaches 1 the end of the run of the wind tunnel is found. The time when this takes place can be found in table 3.4, where it also can be seen that if the throat becomes bigger, the runtime becomes lower. This again is due to a higher mass flow. The run times are still fairly long. This is probably because of the small throats.

One data point for a throat size of 1.676mm with its runtime is highlighted in figure

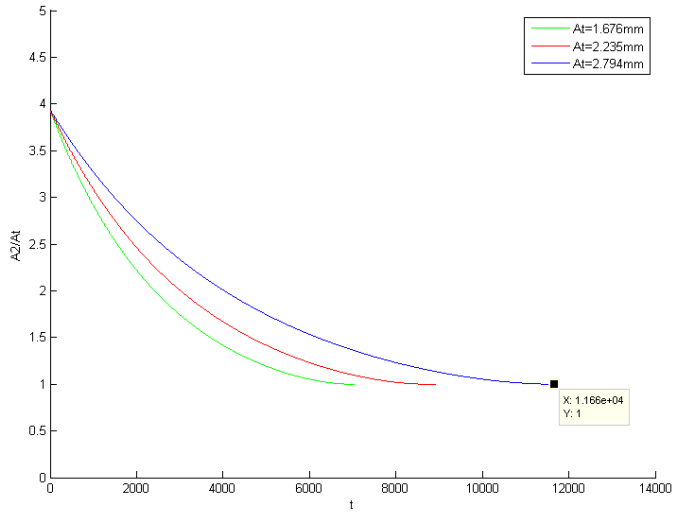

Figure 3.7: Time history of A2/At for $M_1 = 0.85$ for three various throat sizes

3.7. This is the point where the ratio of A_2/A_t is equal to 1. To illustrate the change in A_2 and consequently the change in the pressure ratio and Mach number the figures 3.8a, 3.8b and 3.8c are plotted, for a general converging diverging nozzle. These plots are made with the isentropic relations, so it again is assumed that the nozzle expands ideally, and no shocks are introduced that provide energy losses, energy that cannot be used to entrain the secondary flow. The first portion of the graphs in figure 3.8 stay constant. This is because the geometry is fixed in the first portion of the nozzle (up until the throat). Then when A_2 starts to decrease, the pressure and Mach number start to drop too. The first changes of A_2 result in a small drop, but when the size of A_2 is nearing the throat size A_t, the effect of the change in pressure and Mach number is far greater. This can make it hard to control the tunnel.

	A_t=1.676mm	A_t=2.235mm	A_t=2.794mm
t(s)	11660	8743	6995

Table 3.4: Run lengths for various throat sizes

3.2.1 Optimal area ratio

When the outlet area of the ejector nozzle A_2 and the exit Mach number M_2 get smaller to maintain the same test section Mach number of 0.85, the efficiency of the system drops. The optimal area ratios A_2/A_1 at certain exit Mach numbers that were stated before from Watanawanavet cannot be maintained as can be seen in figure 3.9.

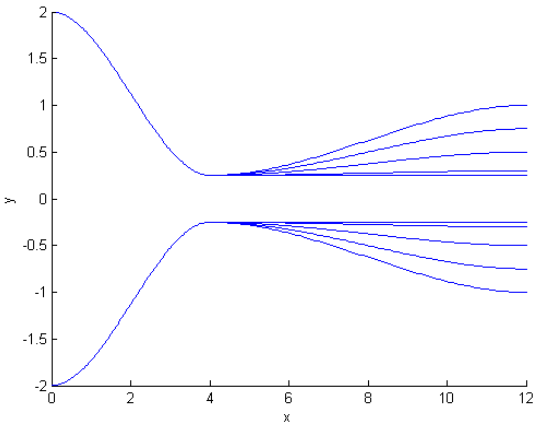

(a) Nozzle geometry with narrowing A_2

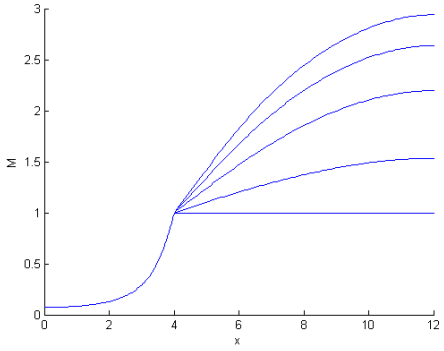

(b) Streamwise variation of the Mach number through the nozzle with changing A_2

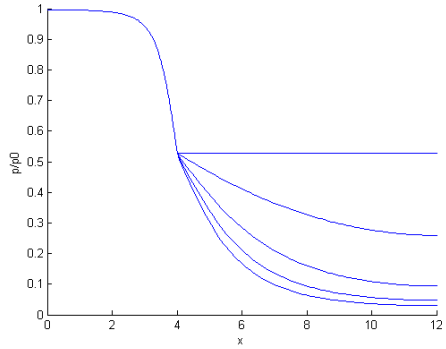

(c) Streamwise variation of the pressure ratio with changing A_2

Figure 3.8: Effect of changing the exit area (A_2) of the nozzle

The optimal ratios described by [6] almost all drop by a factor of roughly 4. This means that the system at the end of the run would be far from the optimal design.

	A_t=1.676mm	A_t=2.235mm	A_t=2.794mm
$(A_2/A_1)_{opt}$	0.03	0.04	0.05
$(A_2/A_1)_{end}$	0.00762	0.0106	0.0127

Table 3.5: Optimal A_2/A_1 and A_2/A_1 at the end of the run

For example, A_2/A_1 changes from 0.05 to 0.013 for the largest throat. At this ratio normally a really high supersonic Mach number ($M >> 3.25$) would be optimal, but in the tunnel the Mach number simultaneously went down to $M_2 = 1$. So it can be assumed that the efficiency has dropped significantly, where at high Mach numbers at

the exit of the ejector the efficiency is already low [6]. In order to check the efficiency, CFD software could be used in this case to see if a better ratio can be found to start out with, so that the overall efficiency during the run drops less.

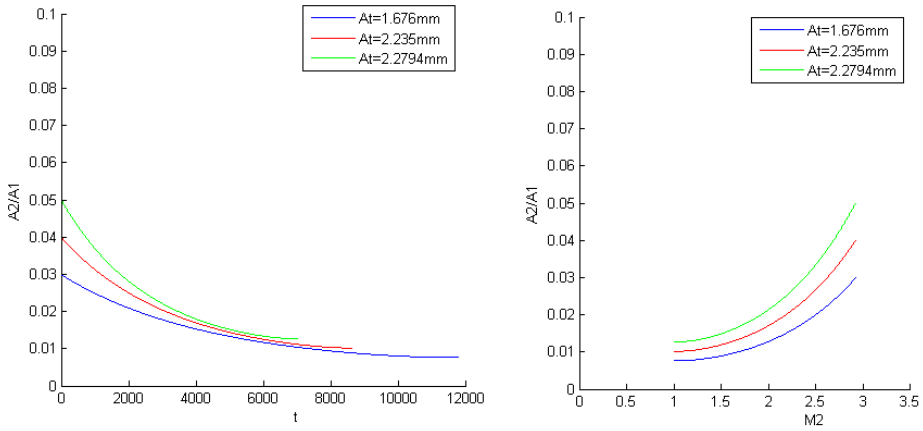

Figure 3.9: Time history of A2/A1 for various throat sizes

4 Computational fluid dynamics

This chapter is about the pre-processor Gridgen and the Computational Fluid Dynamics software Cobalt. These packages would have been used to do simulations in order to get a sufficient design for the induction wind tunnel and ejector system. In this chapter, some dimensions and pointers for the induction tunnel are discussed, which would have been used for the first test case. This can be used in future simulations.

4.1 Gridgen

The pre-processor Gridgen is a software package that is used to generate grids and meshes. It is not limited to any geometry and any geometry can be made. The grids made with Gridgen can be easily be loaded in some CFD software like Cobalt. First a geometry has to be made or loaded into Gridgen (for example with Solidworks). The geometry consists of a database which contains lines and points. Connectors go on top of the database points and lines to define the curve of the grids. Then, to create the actual structured (quadrilateral and hexahedral) or unstructured (triangular and tetrahedral) grid a domain (surface grid) is made. The grid consists out of edges, with the same amount of points (which can be chosen) on the opposite sides for a structured grid, where also the spacing/tolerance of the grid points near a wall can be changed. And lastly the blocks have to be made to group domains and create a volume grid. When the blocks are made, various boundary conditions for different CFD software can be applied on the edges. Multiple blocks can be used to have full control over the mesh grading.

4.1.1 Geometry

The 2D-geometry of the first test case, is a simplified model of the model that can be seen in figure 2.1. To minimize the number of cells and thus the computation time only the above half of the tunnel is used. The induction wind tunnel starts off with a straight section at the beginning of the contraction cone, to ensure that the flow that is coming in is starting as a uniform and horizontal flow. The section is then slowly converged to the size of the test section. This is done with two conic lines in Gridgen, making sure the beginning, end and middle point of the curve are tangent, to have smooth and equal transitions to avoid flow disruptions. The middle point in the contraction is there to adjust the slope and to control the mesh. To avoid any flow separation sharp corners of the tunnel and nozzle are rounded. The slope of the converging part needs to be

shallow enough to avoid adverse pressure gradients, which would be introduced in the first section of the contraction, disrupting the flow. Figure 4.1 displays the geometry, showing the horizontal section and tangent conic lines.

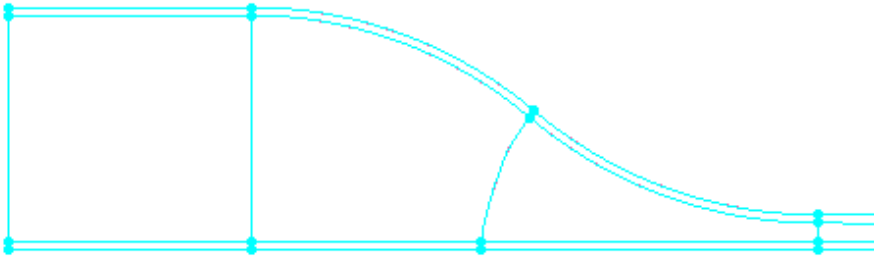

Figure 4.1: Contraction geometry of the first test case

The test section size is then a constant area (with a height of 0.44/2 m), estimated at ten meters long to grow the boundary layer. The length of the test section can be shortened when a sufficient boundary layer growth is reached sooner. This can be checked in future test cases.

An ejector is placed inside the tunnel after the test section. It is placed a little bit above the center line. It is placed inside the tunnel as it has to represent an array of ejectors, that create more shear layers and better mixing than just one on each side of the tunnel [4]. The ejector has the shape of a simple nozzle at first, with a curved line (conic line) in front of the nozzle to avoid flow separation and other anomalies that disrupt the flow (figure 4.2). The mixing section is estimated to be about 2.2 meters long. This is about 5 times the inlet height, which is the least that is needed to ensure completed mixing according to Watanawanavet. In this configuration the mixing section is straight.

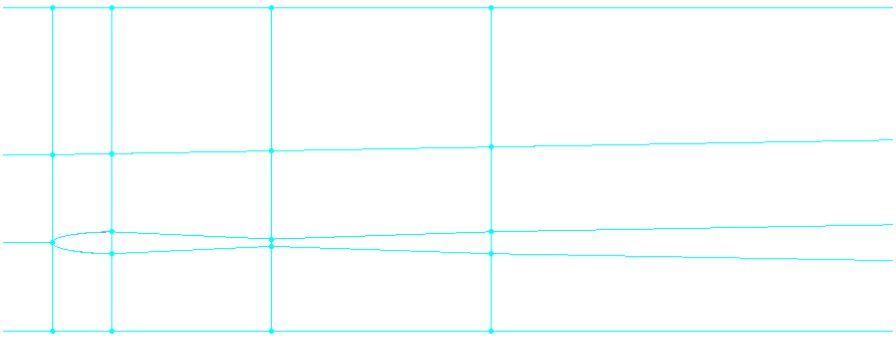

Figure 4.2: Ejector geometry of the first test case

The diffuser starts where the (straight) mixing section has ended. The diffuser needs to

slow the flow down in such a manner that there is good pressure recovery. This means that the included angle of the diffuser should not be too large as the flow would separate from the edge, which gives losses and thus a worse pressure recovery. The included angle should be less than 7.5 degrees [11], which is the chosen angle for this test case. The diffuser should also end again with a horizontal section, so the flow leaves the tunnel in a horizontal way and so that $dp/dn = 0$ at the end of the diffuser, which later can be set as a boundary condition.

4.1.2 Modeling subdomains

To control the mesh and grid locally, extra connectors can be added to create separate subdomains. These subdomains can be edited separately, which means that extra grid points can be added and the grid point distribution can be controlled in that subdomain. This is needed in a boundary layer for example. The (turbulent) boundary layers have high gradients near the wall, where energy is dissipated.

To control the mesh of the boundary layer, an offset line is created below the upper wall of the tunnel. This line, for the first part of the tunnel until the test section, will exactly be the same as the upper part (the actual wall of the tunnel), with an offset of 5 cm at first to capture the turbulent boundary layer. This line is the second line from above in figure 4.1. When the test section starts, the turbulent boundary layer will grow and needs to grow to about 10 cm, this is about the height of the turbulent boundary layer of a modern business jet [7]. To capture this effect of the growing boundary layer in the test section, the newly created line below the upper tunnel wall line also needs to decline. This means that at the beginning of the test section, the boundary layer domain height will be smaller than the height at the end of the test section. It is an iterative process to capture the right height, first layer and expansion of the boundary layer grid, which should be researched in the first few runs. These grid characteristics also depend on the turbulence model that is used.

The shear layers that will exist at the end of the ejector will also grow. Their size and expansion also need to be investigated to capture their influence on the flow. At the upper and lower end of the ejector, a shear layer will grow larger on both sides as can be seen in figures 4.2 and 4.3. The shear layers behind the ejector push everything, including the boundary layer from the test section wall, to the outside. This means two extra lines (connectors) should be added behind the ejector to capture this effect. This results in four different rows of domains behind the ejector. These domains should have a finer grid near the newly created connectors to capture the effects of the shear layer. This is important because it has an effect on the mixing, and as stated before the mixing is important to have a good entrainment of the flow, which greatly determines the efficiency of the induction tunnel.

A horizontal connector is created in front of the ejector, starting from the ejector to

the beginning of the tunnel. This creates a starting point for the flow above and under the ejector. This is necessary, because in the middle of the front part of the ejector, a boundary layer will start to grow on both sides of the ejector. This boundary layer has an effect on the flow and probably on the mixing as well.

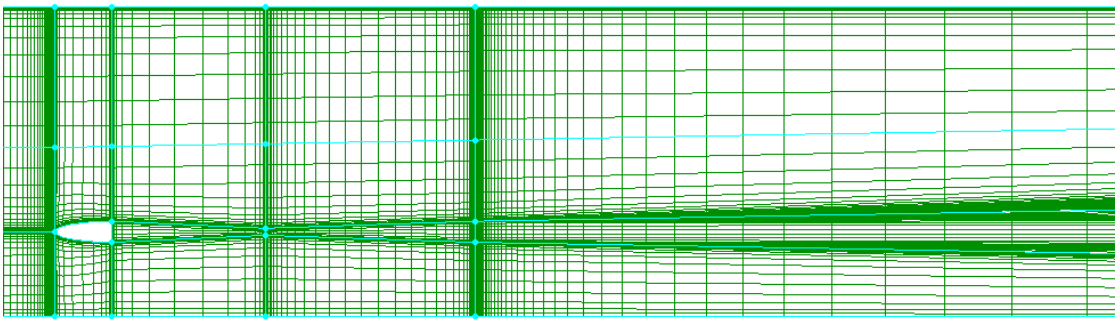

Figure 4.3: Grid distribution near the ejector

A vertical line-connector is placed to create smaller subdomains, wherever the geometry of the wind tunnel or ejector changes direction. With these connectors the mesh can be controlled for each subdomain. The grid will take the shape of the first connector of the domain. This means that the shape of the grid can be made to follow the direction of the flow and to control the number of points. This results in a better mesh, with better smoothness and orthogonality. This is especially helpful near the middle of the contraction of the inlet (the curved line in figure 4.1) and near the ejector (figure 4.3). This way one can also add better grid point spacing near an important part of the wind tunnel like the boundary layer in the test section, the boundary layer on the ejector or the shear layers starting at the end of the ejector.

4.1.3 Grid

There are two types of grids that can be chosen with Gridgen: unstructured grids and structured grids. The grid that is used in the current study is a structured grid, because the geometry is not too complex and with multiple domains/blocks, the grid can be improved locally and manually. A structured grid will give a faster solution than a unstructured grid, as its neighboring points can directly be found via the structure. And generally a structured mesh also needs less cells, which saves memory and time. It will also give a more accurate result, as the aspect ratio is often better than a unstructured grid, in for example a boundary layer where there are large gradients in one direction.

The number of grid points that should be used depends on the complexity of the flow and the aspect ratio because a poor aspect ratio can give convergence errors. When an

analysis is wanted with no slip walls (the actual case), there is going to be a boundary layer. In this boundary layer more points are needed to correctly predict the flow. In the idealized case of the wind tunnel, to first confirm the values of the 1D-analysis, a slip wall (since the ideal situation is calculated in previous chapters) should be used. This means there will be no boundary layer and thus there is no refinement necessary. This will save time for these first computational runs.

In the full test case, with viscosity, a boundary layer with a spacing of 0.000001m is used in vertical direction and a 0.001 spacing in the horizontal direction to have sufficient points to predict a good boundary layer. These spacings give large aspect ratios in the boundary layer, but since the gradients of the boundary layer in the streamwise direction are smaller than the transverse direction this is less of a problem. The rest of the spacing is adjusted so that the grid is smooth with reduced skewness where possible, to maintain the orthogonality.

The aspect ratio of the flow at the inlet and test section is kept at about 50:1 because in these sections a uniform flow is expected, with little change in the flow, thus less points are needed. This speeds up the calculation time. At the ejector the aspect ratio is a lot smaller (around 5:1 or lower) to have more grid points there to capture the flow better and reach convergence.

It should be noted that creating a grid is an iterative process. A study of the meshing size is recommended, by trying for example a course, medium and fine mesh, while keeping in mind that the boundary and shear layers should always have sufficient grid points as this is important to the efficiency of the tunnel.

4.2 Cobalt

The flow solver available was Cobalt. Cobalt is a finite volume, cell centered, 2nd-order accurate in space and time Euler/Navier-Stokes solver. To operate Cobalt it needs a Cobalt input file, a Boundary Condition file and a Grid file. In the input file, the number of processors, gas model, turbulence model and equation set can be set, as well as reference and initial conditions. The grid file from Gridgen needs to be scaled and it's mesh needs to be checked in the Cobalt program Blacksmith. The boundary conditions file is the file where all the boundary conditions can be set.

For the full test cases the turbulent Navier-Stokes equations should be used, as these equations have the most realistic description of the flow. Those equations describe for example boundary layers, viscous dissipation and shock waves.

Cobalt has 12 different turbulence models. Different simulations can be done to check the effect of the different turbulence models on the solution, as different models will

capture different situations like mixing and boundary layers better.

Different boundary conditions need to be set. The initial boundary conditions that were going to be used to test the first simulation used a symmetry plane on the bottom of the tunnel. The reason for this is because the tunnel is believed to be symmetric. This way the upper half is mirrored as the lower half of the tunnel. The upper tunnel wall should be a no-slip wall. This represents a wall where the no-slip condition (velocity at the wall is zero) is satisfied, which means that there will be a boundary layer present on the wall. This is also the case for the walls of the ejector, if the ejector is placed inside the tunnel. This boundary condition can be set to a slip wall when dealing with the ideal case. Then with the so called Riemann invariants boundary condition a total pressure, temperature and direction of the velocity needs to be set at the inlet of the tunnel and the inlet of the nozzle. Finally a total pressure (atmospheric pressure) and exit velocity direction needs to be set at the outlet of the tunnel and the outlet of the ejector.

5 Conclusion and recommendations

Since it was not possible to run CFD simulations during the period of this research at the NRC some one-dimensional wind tunnel analyses were performed.

From the calculations in this report and the literature found, it seems possible to build a working induction wind tunnel with the existing compressor.

However it seems that the high pressure in the storage tanks are not ideal, as this gives very large exit velocities, low entrainment ratios and very small dimensions for the ejector throat according to the calculations. The dimensions calculated for the throat in the ejector seem so small that friction and viscosity (which produces boundary layers) will play a part in the real world.

If the storage tanks with compressed air are used as a source to power the induction wind tunnel they will deplete. This causes the Mach number in the test section to drop. This can be avoided by running the compressor continuously, but that can be rather expensive. Another way is controlling back pressure of the nozzle by changing the throat/exit ratio. This however also changes the ideal expansion, which might introduce shocks and thus losses into the system.

Because the design of an induction wind tunnel is far more complex than a 1D problem it is still recommended to perform CFD calculations. Especially since it is an idealized representation of the real world, where the system in the 1D-analysis is assumed to be reversible and adiabatic. The large differences in velocity and pressure between the primary and secondary stream will almost certainly cause shocks, which will distort the mixing process.

Also all the other effects that are not accounted for in the 1D calculations like turbulence, boundary layers, mixing, heat, different ejector designs and the effect of the sonic throat to prevent sound from traveling upstream need to be investigated and optimized with CFD simulation software.

It is recommended to first validate or compare the CFD model with the ideal 1D-analysis performed in this report, with the available CFD tools. After that the other features like the sonic throat and different type of ejectors can be added to see the effect they have on the flow.

A parameter study of a 2D- and eventually a 3D-model of an induction tunnel with different ejector designs and dimensions should be made, to closely monitor the effect on

the performance. Various turbulence models need to be tested that represent the complex boundary layers and mixing of the flow through the tunnel as realistic as possible.

5.1 Alternative ejector designs

Since it was not possible to simulate and test the different ejector designs with CFD, some recommendations of promising ejector designs are discussed. The different ejector designs that could make the system more efficient are ejectors that make use of the Candoa effect, guide vanes, constant rate of momentum, a chevron nozzle or petal nozzles. It is also possible that a combination of these designs make an even better system for the wind tunnel. They will be briefly discussed below.

5.1.1 Chevron Nozzle

Chevron nozzles are widely used in the aerospace science and aircraft engines already. They have many advantages like noise reduction and they also improve the standard normal converging-diverging nozzle. H.D. Kim et al. [12] also mention that a chevron nozzle makes more longitudinal vortices. These longitudinal vortices involve more secondary stream into the ejector by transferring more energy between the primary and the entrained flow. This way the mixing process was enhanced. The entrainment ratio in the paper mentioned was increased by 15 percent with a maximum of 22 percent with using a 10 chevron nozzle (see figure 5.1). The pressure recovery was also increased on average by 9 percent.

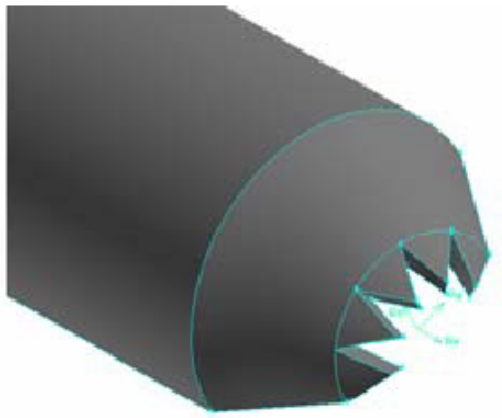

Figure 5.1: Chevron nozzle [12]

5.1.2 Petal Nozzle

The petal nozzle (figure 5.2) can also be used to improve the nozzle performance. Petal nozzles are also widely used in the aerodynamic field to reduce jet noise and increase the trust force. However, they can also be used to enhance the mixing process by creating better streamwise vorticity due to the flow shedding periodically from the trailing edge. Y.J. Chang [13] showed that petal nozzles in combination with a large area ratio between a constant mixing area section (A_3) and the nozzle throat (A_t) have better performance than just a conical nozzle. This idea should be tested with CFD to see if it gives a better performance than the chevron nozzle for the induction tunnel.

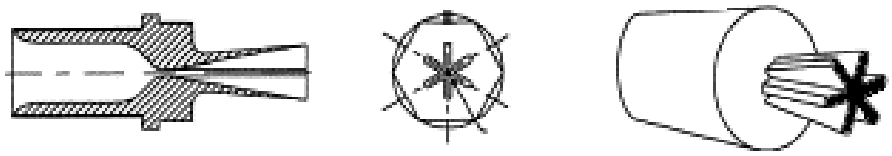

Figure 5.2: Petal nozzle [13]

5.1.3 Constant Rate of Momentum Change (CRMC)

Apart from frictional losses, mixing losses and kinetic energy losses there are usually also shocks involved with an induction tunnel, because of the large pressure and velocity gradients. These shocks are a large impediment towards designing an efficient supersonic ejector and thus a wind tunnel in this case. The idea of a constant rate momentum change ejector is to have a mixing section that gradually becomes bigger (like a diffuser), instead of a constant pressure or constant area mixing section mentioned in the beginning of this report. The slightly increasing area needs to keep the momentum change at a constant rate, which allows the pressure to rise gradually from begin to exit, which avoids or minimizes shocks [14] and total pressure losses. A comparison of the pressures between a conventional and CRMC mixing section can be found in figure 5.3. K. Palani [15] shows that the entrainment ratio almost increases 50 percent by using the CRMC method compared to the conventional (constant area) model. This looks very promising and should be investigated through CFD to investigate if this is also the case for the induction wind tunnel at even higher velocities.

5.1.4 Mixing guide vanes

Mixing guide vanes are vanes, that for example, are shaped like an airfoil. These vanes are installed inside the tunnel. Multiple vanes above each other of different lengths can be installed. They must be installed in such a way that when the primary and secondary flow meet they have the similar velocities. This way the energy transfer between the streams is increased and this in turn increases the efficiency of the ejector

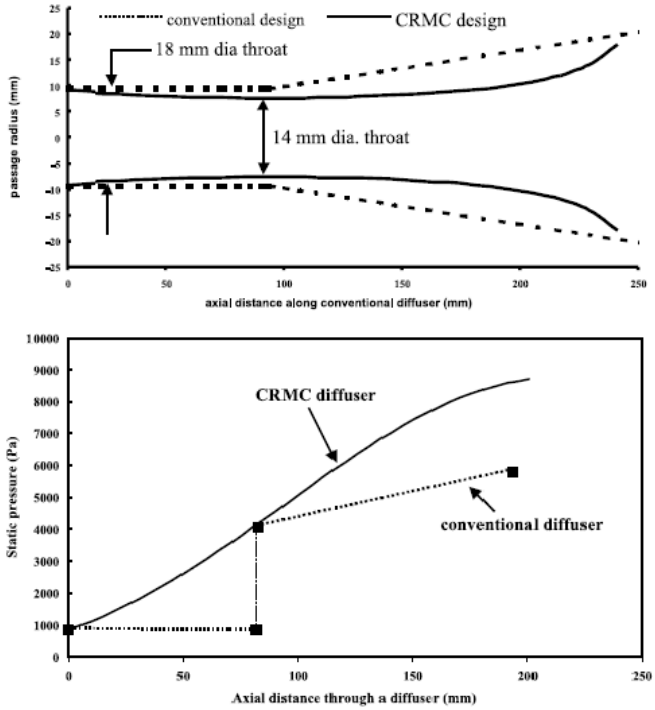

Figure 5.3: Pressure loss of a conventional and CRMC ejector [14]

[10]. The number, shapes and the lengths of these vanes should be investigated as the optimum can be different for different Mach numbers. H.D. Kim [16] mentions that the entrainment ratio was improved by 7.5 percent as the maximum value and a maximum increment of pressure recovery of 37 percent for their optimal design.

5.1.5 Coanda effect

The Coanda effect is the ability of a flow to follow a curved contour without separation. The primary flow out of the ejector/nozzle follows an optimal curvature and entrains the secondary stream better due to the momentum transfer between the two. The effect has already been employed in aerospace applications for a long time and is known to improve the performances of various devices [17]. This effect is also used in air amplifiers from the company Nex Flow for example. They mention they entrain flow with up to an amplifications of 17 times the airflow, depending on the size of the device [18] due to the Coanda effect. This looks like a promising enhancement and should be tested with CFD software. The injector for example can be placed on the side of the first throat, where a curvature is present, or a curvature can be made where the compressed flow enters the tunnel. This is a possibility to make a system that entrains more flow and thus has a better entrainment ratio.

5.1.6 Jet engine

The option of using a Jet engine instead of a compressor for driving the primary fluid is also available, as the NRC may have one available, which reduces investment costs. With using a jet a more continuous flow can be created. However, using a Jet instead of a compressor a lot of different factors come in play, namely the exhaust and its temperature.

5.1.7 Array/cluster of nozzles

The idea of an array or cluster of nozzles inside the tunnel should also be investigated. By having multiple jets inside the tunnel it is believed that more longitudinal vortices and shear layers are created which will also help to entrain the flow.

Appendix A

Derivations

A.1 Pressure ratio

The one-dimensional flow through the tunnel is considered compressible, steady, isentropic and thus non-viscous and non-heat-conducting. If then a finite portion V of the tunnel is considered where the surface is represented by $S = \partial V$ where the unit normal vector $\vec{n}$ on the surface is positive pointing out of the control volume V. The density is represented by $\rho(x)$, the velocity by $\vec{u}(x)$ and the pressure by $p(x)$, where x is a position on the x-axis located along the axis of the tunnel. H is the total enthalpy $H = h + \frac{1}{2}u^2 = E + p/\rho$.

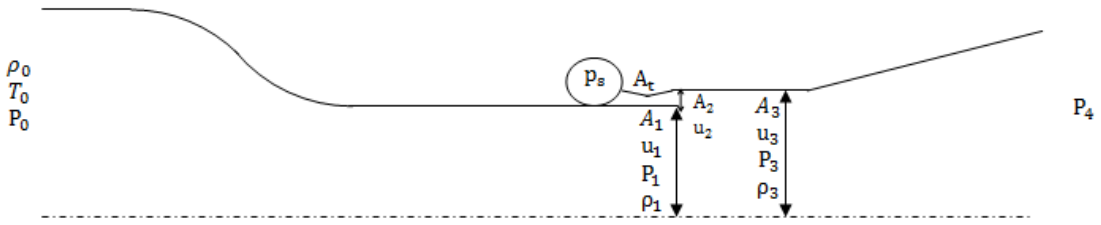

Figure A.1: Simplified one-dimensional tunnel

Since the mixing section is constant, the areas can be related through the following equations.

$$A_3 = A_2 + A_1 \tag{A.1}$$

$$\frac{A_2}{A_3} << 1 \tag{A.2}$$

The cross-sectional area of the channel or the stream tube is A(x). The area at the test section, exit of the nozzle and the mixing section are denoted by A_1, A_2 and A_3 respectively.

The three conservation equations that describe the flow through the tunnel are described below starting from the integral conservation form.

Conservation of Mass:

$$\iint_{\partial V} \rho \vec{u} \cdot \vec{n} dS = 0 \tag{A.3}$$

$$A_3 u_3 \rho_3 = A_2 u_2 \rho_2 + A_1 u_1 \rho_1 \tag{A.4}$$

$$\dot{m}_3 = \dot{m}_2 + \dot{m}_1 \tag{A.5}$$

Conservation of Momentum:

$$\iint_{\partial V} (\rho u(\vec{u} \cdot \vec{n}) + p(\vec{n} \cdot \vec{e}_x)) dS = 0 \tag{A.6}$$

$$p_1 A_1 + p_2 A_2 - p_3 A_3 = A_3 u_3^2 \rho_3 - (A_2 u_2^2 \rho_2 + A_1 u_1^2 \rho_1) \tag{A.7}$$

$$p_1 (A_1 + A_2) - p_3 A_3 = A_3 u_3^2 \rho_3 - (A_2 u_2^2 \rho_2 + A_1 u_1^2 \rho_1) \tag{A.8}$$

$$A_3 (p_1 - p_3) = A_3 u_3^2 \rho_3 - (A_2 u_2^2 \rho_2 + A_1 u_1^2 \rho_1) \tag{A.9}$$

At the end of the ejector p_2 and p_1 are taken the same. If this is not the case, nature will introduce shock waves to match the pressure of p_2 and p_1. That is why the nozzle of the ejector is assumed to expand isentropically until the primary and secondary streams have the same pressure, so there are no shock waves. This means that p_2 and p_1 are assumed the same pressure before any mixing takes place at the exit of the nozzle.

Conservation of Energy:

$$\iint_{\partial V} \rho H(\vec{u} \cdot \vec{n}) dS = 0 \tag{A.10}$$

$$(h_3 + \frac{u_3^2}{2}) \rho_3 u_3 A_3 = (h_1 + \frac{u_1^2}{2}) \rho_1 u_1 A_1 + (h_2 + \frac{u_2^2}{2}) \rho_2 u_2 A_2 \tag{A.11}$$

which is equal to

$$(C_p T_3 + \frac{u_3^2}{2}) \rho_3 u_3 A_3 = (C_p T_1 + \frac{u_1^2}{2}) \rho_1 u_1 A_1 + (C_p T_2 + \frac{u_2^2}{2}) \rho_2 u_2 A_2 \tag{A.12}$$

With $T = \frac{P}{\rho R}$, $C_p - C_v$ and $\gamma = C_p / C_v$ this can be rewritten to

$$\left(\frac{\gamma}{(\gamma - 1)} \frac{p_3}{\rho_3} + \frac{u_3^2}{2} \right) \rho_3 u_3 A_3 = \left(\frac{\gamma}{(\gamma - 1)} \frac{p_1}{\rho_1} + \frac{u_1^2}{2} \right) \rho_1 u_1 A_1 + \left(\frac{\gamma}{(\gamma - 1)} \frac{p_2}{\rho_2} + \frac{u_2^2}{2} \right) \rho_2 u_2 A_2 \tag{A.13}$$

It is assumed that the stagnation temperature is the same for the compressed air supply and the induced air. And since the tunnel and nozzle are assumed to be irreversible and isentropic this leads to

$$\frac{\gamma}{(\gamma-1)}\frac{p_3}{\rho_3}+\frac{u_3^2}{2}=\frac{\gamma}{(\gamma-1)}\frac{p_2}{\rho_2}+\frac{u_2^2}{2}=\frac{\gamma}{(\gamma-1)}\frac{p_1}{\rho_1}+\frac{u_1^2}{2}=C \tag{A.14}$$

u_3 can now be written with the help of equation A.5 as

$$u_3^2+\frac{2\gamma}{\gamma-1}\frac{u_3A_3p_3}{(\dot{m}_1+\dot{m}_2)}-2C=0 \tag{A.15}$$

$$u_3=-\frac{\gamma}{(\gamma-1)}\frac{A_3p_3}{(\dot{m}_1+\dot{m}_2)}\pm\sqrt{\frac{\gamma^2}{(\gamma-1)^2}\left(\frac{A_3p_3}{(\dot{m}_1+\dot{m}_2)}\right)^2+2C} \tag{A.16}$$

Equation A.9 can then be rewritten with the help of the continuity equation to

$$p_1-p_3=\frac{(\dot{m}_1+\dot{m}_2)u_3}{A_3}-\frac{(\dot{m}_1u_1+\dot{m}_2u_2)}{A_3} \tag{A.17}$$

Then u_3 (equation A.16) is filled in and a lot of algebra is applied, p_3 is obtained:

$$p_1-p_3=\frac{(\dot{m}_1+\dot{m}_2)}{A_3}\left(-\frac{\gamma}{(\gamma-1)}\frac{A_3p_3}{(\dot{m}_1+\dot{m}_2)}\pm\sqrt{\frac{\gamma^2}{(\gamma-1)^2}\left(\frac{A_3p_3}{(\dot{m}_1+\dot{m}_2)}\right)^2+2C}\right)..$$
$$-\frac{(\dot{m}_1u_1+\dot{m}_2u_2)}{A_3} \tag{A.18}$$

$$p_1-p_3=-\frac{p_3\gamma}{(\gamma-1)}\pm\sqrt{\frac{p_3^2\gamma^2}{(\gamma-1)^2}+2C\left(\frac{(\dot{m}_1+\dot{m}_2)}{A_3}\right)^2}-\frac{(\dot{m}_1u_1+\dot{m}_2u_2)}{A_3} \tag{A.19}$$

$$p_1-\frac{p_3(\gamma-1)}{\gamma-1}+\frac{p_3\gamma}{(\gamma-1)}=\pm\sqrt{\frac{p_3^2\gamma^2}{(\gamma-1)^2}+2C\left(\frac{(\dot{m}_1+\dot{m}_2)}{A_3}\right)^2}-\frac{(\dot{m}_1u_1+\dot{m}_2u_2)}{A_3} \tag{A.20}$$

rearranging the terms and squaring them gives

$$\left(p_1 + \frac{p_3}{(\gamma-1)} + \frac{(\dot{m}_1 u_1 + \dot{m}_2 u_2)}{A_3}\right)^2 = \left(\pm\sqrt{\frac{p_3^2\gamma^2}{(\gamma-1)^2} + 2C\left(\frac{(\dot{m}_1+\dot{m}_2)}{A_3}\right)^2}\right)^2 \tag{A.21}$$

$$\frac{p_3^2}{(\gamma-1)^2} + \frac{2p_3}{(\gamma-1)}\left(p_1 + \frac{(\dot{m}_1 u_1 + \dot{m}_2 u_2)}{A_3}\right) + \left(p_1 + \frac{(\dot{m}_1 u_1 + \dot{m}_2 u_2)}{A_3}\right)^2 \tag{A.22}$$
$$= \frac{p_3^2\gamma^2}{(\gamma-1)^2} + 2C\left(\frac{(\dot{m}_1+\dot{m}_2)}{A_3}\right)^2$$

Collecting the terms to one side and multiply every term with $\frac{\gamma-1}{\gamma+1}$ yields

$$p_3^2 - \frac{2}{(\gamma+1)}\left(p_1 + \frac{(\dot{m}_1 u_1 + \dot{m}_2 u_2)}{A_3}\right)p_3 - \frac{\gamma-1}{\gamma+1}\left(p_1 + \frac{(\dot{m}_1 u_1 + \dot{m}_2 u_2)}{A_3}\right)^2 \tag{A.23}$$
$$+2C\frac{\gamma-1}{\gamma+1}\left(\frac{(\dot{m}_1+\dot{m}_2)}{A_3}\right)^2 = 0$$

When the quadratic formula is used p_3 can be found. Taking

$$Z = \left(p_1 + \frac{(\dot{m}_1 u_1 + \dot{m}_2 u_2)}{A_3}\right) \tag{A.24}$$

to simplify the equation, since it occurs multiple times. Leads to

$$\frac{1}{(\gamma+1)}Z \pm \frac{1}{\sqrt{4}}\sqrt{\frac{4}{(\gamma+1)^2}Z^2 - 4\left(-\frac{\gamma-1}{\gamma+1}\frac{\gamma+1}{\gamma+1}Z^2 + 2C\frac{\gamma-1}{\gamma+1}\left(\frac{(\dot{m}_1+\dot{m}_2)}{A_3}\right)^2\right)} \tag{A.25}$$

Filling everything back in and taking the first two terms in the root together the following is obtained

$$p_3 = \frac{1}{(\gamma+1)}\left[p_1 + \left(\frac{\dot{m}_1 u_1 + \dot{m}_2 u_2}{A3}\right)\right] \tag{A.26}$$
$$\pm\sqrt{\frac{\gamma^2}{(\gamma+1)^2}\left[p_1 + \left(\frac{\dot{m}_1 u_1 + \dot{m}_2 u_2}{A3}\right)\right]^2 - 2C\frac{(\gamma-1)}{(\gamma+1)}\left(\frac{\dot{m}_1+\dot{m}_2}{A_3}\right)^2}$$

Dividing the above equation by p_1 on both sides and by replacing the following relations:

$$\dot{m}_1 u_1 = A_1\rho_1 u_1^2 \tag{A.27}$$

$$\frac{\dot{m}_1 u_1}{p_1} = \frac{A_1\rho_1 u_1^2}{p_1}\frac{\gamma}{\gamma} = \frac{A_1 u_1^2\gamma}{a^2} = \gamma A_1 M_1^2 \tag{A.28}$$

and for C with constant total temperature and the sonic point as a reference, $u = a^*$ with $a^2 = \gamma RT = \gamma \frac{p}{\rho}$ and $\frac{T^*}{T_0} = \frac{2}{\gamma+1}$.

From the incompressible Bernoulli relation

$$\frac{1}{2}u^2 + \int \frac{dp}{\rho} \tag{A.29}$$

and the Poisson relation ($p = C\rho^\gamma$) it follows for an isentropic flow with a calorically perfect gas that $\frac{a^2}{\gamma-1} = c_p T$ [8]. And thus

$$\frac{1}{2}u^2 + \frac{a^2}{\gamma-1} = \frac{1}{2}a^{*2} + \frac{a^{*2}}{\gamma-1} = \frac{a_0^2}{\gamma-1} \tag{A.30}$$

$$\frac{\gamma-1}{2(\gamma-1)}a^{*2} + \frac{2a^{*2}}{2(\gamma-1)} = \frac{\gamma+1}{2(\gamma-1)}a^{*2} \tag{A.31}$$

Which leads to the following relation for the constant C

$$C = \frac{\gamma}{(\gamma-1)}\frac{p_3}{\rho_3} + u_3^2/2 = \frac{1}{(\gamma-1)}\frac{\gamma p_0}{\rho_0} + u_0^2/2 = \frac{a_0^2}{(\gamma-1)} = \frac{\gamma+1}{2(\gamma-1)}a^{*2} \tag{A.32}$$

where the stagnation velocity $u_0 = 0$ by definition.

Filling this in in equation p_3, dividing by p_1 together with equation A.29 gives

$$\frac{p_3}{p_1} = \frac{1}{(\gamma-1)}\left(1 + \gamma\frac{A_1M_1^2 + A_2M_2^2}{A_3}\right) \tag{A.33}$$
$$\pm\sqrt{\frac{\gamma^2}{(\gamma+1)^2}\left(1+\gamma\frac{A_1M_1^2+A_2M_2^2}{A_3}\right)^2 - \gamma^2 a^{*2}\left(\frac{A_1M_1^2}{u_1A_3} + \frac{A_2M_2^2}{u_2A_3}\right)^2}$$

$$\frac{p_3}{p_1} = \frac{1}{(\gamma-1)}\left(1 + \gamma\frac{M_1^2 + \frac{A_2}{A_1}M_2^2}{(1+\frac{A_2}{A_1})}\right) \tag{A.34}$$
$$\pm\gamma\sqrt{\frac{\gamma^2}{(\gamma+1)^2}\left(1+\gamma\frac{M_1^2+\frac{A_2}{A_1}M_2^2}{(1+\frac{A_2}{A_1})}\right)^2 - \left(\frac{a^*M_1^2}{u_1(1+\frac{A_2}{A_1})} + \frac{\frac{A_2}{A_1}a^*M_2^2}{u_2(1+\frac{A_2}{A_1})}\right)^2}$$

where only the pressure ratio with the positive second term gives physical answers. This pressure ratio is plotted in figure A.2.

Equation A.16 can now also be completed with C which leads to

$$u_3 = -\frac{\gamma}{(\gamma-1)}\frac{A_3p_3}{(\dot{m}_1+\dot{m}_2)} \pm \sqrt{\frac{\gamma^2}{(\gamma-1)^2}\left(\frac{A_3p_3}{(\dot{m}_1+\dot{m}_2)}\right)^2 + \frac{\gamma+1}{(\gamma-1)}a^{*2}} \tag{A.35}$$

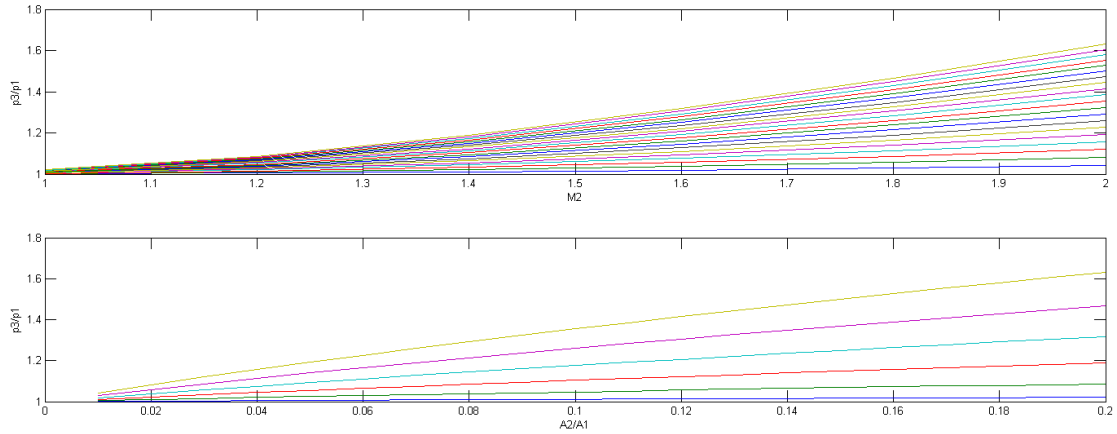

Figure A.2: Top figure shows $\frac{p_3}{p_1}$ vs M_2 for different area ratios of $\frac{A_2}{A_1}$.
Bottom figure shows $\frac{p_3}{p_1}$ vs $\frac{A_2}{A_1}$ for different M_2. Both at constant $M_1 = 0.85$

A.2 Isentropic relations

p_1/p_0 and p_4/p_3 can be evaluated through the isentropic relations listed below:

$$\frac{p_0}{p} = \left(1 + \frac{\gamma - 1}{2} M^2\right)^{\frac{\gamma}{\gamma - 1}} \tag{A.36}$$

$$\frac{T_0}{T} = \left(1 + \frac{\gamma - 1}{2} M^2\right) \tag{A.37}$$

$$\frac{\rho_0}{\rho} = \left(1 + \frac{\gamma - 1}{2} M^2\right)^{\frac{1}{\gamma - 1}} \tag{A.38}$$

A.3 M_3

M_3 can be calculated by obtaining u_3 from equation A.35 and dividing it by a^*. With the help of equation A.30 and remembering that $M = \frac{u}{a}$ one obtains

$$\frac{1}{2} + \frac{a_3^2}{u_3^2(\gamma-1)} = \frac{\gamma+1}{2(\gamma-1)}\frac{a^{*2}}{u_3^2} \tag{A.39}$$

$$\frac{1}{2} + \frac{1}{M_3^2(\gamma-1)} = \frac{\gamma+1}{2(\gamma-1)}\frac{a^{*2}}{u_3^2} \tag{A.40}$$

$$\left(\frac{u_3}{a^*}\right)^2 = M^{*2} = \frac{\gamma+1}{\gamma-1+\frac{2}{M_3^2}} \tag{A.41}$$

$$M_3^2 = \frac{2}{\frac{\gamma+1}{\left(\frac{u_3}{a^*}\right)^2} - \gamma + 1} \tag{A.42}$$

A.4 Mass flow through the throat

The mass flow through the throat of the nozzle can be calculated with the following formula [8].

$$\dot{m}_t = \rho_t A_t u_t = A_t \sqrt{\frac{2\gamma}{\gamma-1} p_s \rho_s \left[\left(\frac{p_t}{p_s}\right)^{\frac{2}{\gamma}} - \left(\frac{p_t}{p_s}\right)^{\frac{\gamma+1}{\gamma}}\right]} \tag{A.43}$$

which can be rewritten to

$$\dot{m}_t = \rho_t A_t u_t = A_t \sqrt{\frac{2\gamma}{\gamma-1}\left(\frac{\rho_t}{\rho_s}\right)^2 p_s \rho_s \left[1 - \left(\frac{p_t}{p_s}\right)^{\frac{\gamma-1}{\gamma}}\right]} \tag{A.44}$$

with the mass flow being maximum for $\gamma = 1.4$ at the throat at

$$\frac{p}{p_s} = \left(\frac{2}{\gamma+1}\right)^{\frac{\gamma}{\gamma-1}} = 0.5283 \tag{A.45}$$

so the equation for the maximum mass flow becomes

$$\dot{m}_{t,max} = A^* \sqrt{\frac{2\gamma}{\gamma-1}\left(\frac{2}{\gamma+1}\right)^{\frac{2\gamma}{\gamma-1}} \rho_0 p_0 \left(\frac{\gamma+1}{\gamma+1} - \frac{2}{\gamma+1}\right)} \tag{A.46}$$

$$\dot{m}_{t,max} = A^* \sqrt{p_s \rho_s} \sqrt{\frac{2\gamma}{\gamma+1}} \left(\frac{2}{\gamma+1}\right)^{\frac{1}{\gamma-1}} \tag{A.47}$$

$$p_s = \rho_s R T_s \tag{A.48}$$

A.5 Blow down time of the storage tank

The mass flow leaving the tank can be calculated with the perfect gas law

$$p = \frac{m}{V} RT \tag{A.49}$$

$$pV = mRT \tag{A.50}$$

and differentiating $T(t)$, $P(t)$ and $m(t)$ with respect to time

$$V\frac{dp}{dt} = mR\frac{dT}{dt} + RT\frac{dm}{dt} \tag{A.51}$$

For an isentropic flow the following relation is valid (Poisson's relation)

$$p = C\rho^{\gamma} \tag{A.52}$$

$$p^{\frac{1}{\gamma}}\frac{RT}{p} = C \tag{A.53}$$

$$p^{\frac{1-\gamma}{\gamma}}T = \frac{C}{R} = C' \tag{A.54}$$

Differientating the natural logarithm of both sides gives

$$\frac{1-\gamma}{\gamma}\frac{dp}{p} + \frac{dT}{T} = 0 \tag{A.55}$$

and thus T changes in time according to

$$\frac{dT}{dt} = \frac{\gamma - 1}{\gamma}\frac{T}{p}\frac{dp}{dt} \tag{A.56}$$

Now using a transformed equation of the maximum massflow where it is assumed that the throat is choked at all times with a minus sign, because the flow is leaving the tank

$$\dot{m} = \frac{dm}{dt} = \frac{-pA^*}{\sqrt{T}}\sqrt{\frac{\gamma}{R}}\sqrt{\left(\frac{2}{\gamma+1}\right)^{\frac{\gamma+1}{\gamma-1}}} \tag{A.57}$$

Filling it in in the perfect gas law, equation A.51, gives

$$V\frac{dp}{dt} = mR\left(\frac{T}{p}\frac{\gamma-1}{\gamma}\frac{dp}{dt}\right) - RT\left[\frac{pA^*}{\sqrt{T}}\sqrt{\frac{\gamma}{R}\left(\frac{2}{\gamma+1}\right)^{\frac{\gamma+1}{\gamma-1}}}\right] \tag{A.58}$$

and from Poisson's relation and the isentropic relations one obtains

$$T = T_i\frac{p}{p_i}^{\frac{(\gamma-1)}{\gamma}} \tag{A.59}$$

where T_i and p_i are the initial (and thus stagnation) conditions in the tank. Then with

$$V = \frac{mRT}{p} \tag{A.60}$$

equation A.58 becomes

$$-V\frac{dp}{dt}\left(1 - \frac{\gamma - 1}{\gamma}\right) = R\sqrt{T_i}\left(\frac{p}{p_i}\right)^{\frac{\gamma-1}{2\gamma}} pA^*\sqrt{\frac{\gamma}{R}\left(\frac{2}{\gamma+1}\right)^{\frac{\gamma+1}{\gamma-1}}} \tag{A.61}$$

$$\frac{dp}{dt} = -\left[\frac{A^*R\sqrt{T_i}}{p_i^{\frac{\gamma-1}{2\gamma}}}\frac{\gamma}{V}\sqrt{\frac{\gamma}{R}\left(\frac{2}{\gamma+1}\right)^{\frac{\gamma+1}{\gamma-1}}}\right] p^{\frac{3\gamma-1}{2\gamma}} \tag{A.62}$$

Now using separation of variables this becomes

$$\int_{p_i}^{p_s} p^{\frac{1-3\gamma}{2\gamma}}\, dp = -\left[\frac{A^*R\sqrt{T_i}}{p_i^{\frac{\gamma-1}{2\gamma}}}\frac{\gamma}{V}\sqrt{\frac{\gamma}{R}\left(\frac{2}{\gamma+1}\right)^{\frac{\gamma+1}{\gamma-1}}}\right]\int_0^t dt \tag{A.63}$$

where p_s now denotes the (depleting) pressure in the tank. After integrating equation A.63, a function for the time can be found:

$$t = \frac{-1}{\left[\frac{A^*R\sqrt{T_i}}{p_i^{\frac{\gamma-1}{2\gamma}}}\frac{\gamma}{V}\sqrt{\frac{\gamma}{R}\left(\frac{2}{\gamma+1}\right)^{\frac{\gamma+1}{\gamma-1}}}\right]}\frac{2\gamma}{1-\gamma}\left(p_s^{\frac{1-\gamma}{2\gamma}} - p_i^{\frac{1-\gamma}{2\gamma}}\right) \tag{A.64}$$

$$t = \frac{-2V}{\left[A^*R\sqrt{T_i}\sqrt{\frac{\gamma}{R}\left(\frac{2}{\gamma+1}\right)^{\frac{\gamma+1}{\gamma-1}}}\right](1-\gamma)}\left[\left(\frac{p_s}{p_i}^{\frac{1-\gamma}{2\gamma}}\right) - 1\right] \tag{A.65}$$

which can also be rewritten to $p_s(t)$:

$$p_s(t) = \left(\frac{t\cdot(1-\gamma)R\sqrt{T_i}A_t\sqrt{\frac{\gamma}{R}\left(\frac{2}{\gamma+1}\right)^{\frac{\gamma+1}{\gamma-1}}}}{-2V} + 1\right)^{\frac{2\gamma}{1-\gamma}} \cdot p_i \tag{A.66}$$

Appendix B

Matlab

B.1 Wind_tunnel_calculations.m

```
%%%%%%%%%%%%%%%%%%%%%%%%%%%%%%%%%%%%%%%%%%%%%%%%%%%%%%%%%%%%%%%%%%%%%%%%%%%%%%%%
% Wind tunnel calculations
%%%%%%%%%%%%%%%%%%%%%%%%%%%%%%%%%%%%%%%%%%%%%%%%%%%%%%%%%%%%%%%%%%%%%%%%%%%%%%%%
%
% Author: D.G.J. Detert Oude Weme
%
% Modified: 23-09-2014
%
%%%%%%%%%%%%%%%%%%%%%%%%%%%%%%%%%%%%%%%%%%%%%%%%%%%%%%%%%%%%%%%%%%%%%%%%%%%%%%%%
%
% Inputs
%
%%%%%%%%%%%%%%%%%%%%%%%%%%%%%%%%%%%%%%%%%%%%%%%%%%%%%%%%%%%%%%%%%%%%%%%%%%%%%%%%
%clear and close screen and workspace
close all
clear all
clc

g=1.40 %Gamma
deff=1 %Diffuser efficiency
T0=298 %temperature (K) throughout the tunnel
R=287 %gasconstant (J/kgK)
astar=sqrt(2/(g+1)*g*R*T0) %Local speed of sound
p0=101325  %atmospheric pressure (Pa)
ps=2068427.19 %pressure compressor (Pa), 300 psi
rs=ps/(R*T0) %rho compressor (kg/m3)
l=ps/p0 %compression ratio compressor/atmosphere ps/p0
%l=2.1
M1=0.00:0.05:0.85; %Test section mach number range
A2A1=0.03:0.01:0.05; %Area ratio A2/A1 range 0.03:0.01:0.05
pps=0.528 %pressure ratio throat/ps
A2=0.0066 %0.0066, 0.0088, 0.011
%%%%%%%%%%%%%%%%%%%%%%%%%%%%%%%%%%%%%%%%%%%%%%%%%%%%%%%%%%%%%%%%%%%%%%%%%%%%%%%%
%
%Calculations: loops and equations
%
```

```
%%%%%%%%%%%%%%%%%%%%%%%%%%%%%%%%%%%%%%%%%%%%%%%%%%%%%%%%%%%%%%%%%%%%%%%%%%%%

for i=1:length(M1)
        M2(i)=sqrt((l^((g-1)/g)*2*(1+(g-1)/2*M1(i)^2)-2)/(g-1));
        A2At(i)=sqrt(1/M2(i)^2*((2/(g+1))*(1+(g-1)/2*M2(i)^2))^((g+1)/(g...
            -1)));
        asu1(i)=sqrt((g-1+2/(M1(i)^2))/(g+1));
        asu2(i)=sqrt((g-1+2/(M2(i)^2))/(g+1));
        p1p0(i)=1/((1+(g-1)/2*M1(i)^2)^(g/(g-1)));
        p1(i)=p1p0(i)*p0;
        MF(i)=2*A2*(1/A2At(i))*(sqrt((2*g)/(g-1)*ps*rs*(pps^(2/g)-pps^((g...
            +1)/g))));   %massflow/A2

        for j=1:length(A2A1)
            AtA3(i,j)=(1/(1/(A2A1(j))+1))*(1/(A2At(i)));
                term1(i,j)=1/(1+g)+(g/(1+g))*((M1(i)^2+M2(i)^2*A2A1(j))...
                    /(1+A2A1(j)));
                term3(i,j)=(M1(i)^2*asu1(i)+ M2(i)^2*A2A1(j)*asu2(i))/(1+...
                    A2A1(j));

term1a(i,j)=1/(1+g)+(g/(1+g))*((M1(i)^2+M2(i)^2*A2A1(j))/(1+A2A1(j)));
term3a(i,j)=(M1(i)^2*(sqrt((g-1+(2/M1(i)^2))/(g+1)))+ M2(i)^2*A2A1(j)*(...
    sqrt((g-1+(2/M2(i)^2))/(g+1) )))/(1+A2A1(j));

                p3p1m(i,j)= term1(i,j)-g*(sqrt((term1(i,j))^2-(term3(i,j)...
                    )^2)); %Nonphysical answers
                p3p1p(i,j)= term1(i,j)+g*(sqrt((term1(i,j))^2-(term3(i,j)...
                    )^2)); %plus sign

p3p1a(i,j)= term1a(i,j)+g*(sqrt((term1a(i,j))^2-(term3a(i,j))^2));%P3/P1 ...
    without a* in it, gives the same answers as p3p1p

                    term1a(i,j)=-1/(g-1)*(p3p1p(i,j))*(1+A2A1(j))/((M1(i)...
                        ^2*asu1(i))+(M2(i)^2*asu2(i)*(A2A1(j))));
                    term2a(i,j)=1/((g-1)^2)*(p3p1p(i,j))^2*((1+A2A1(j))/((...
                        M1(i)^2*asu1(i))+(M2(i)^2*asu2(i)*(A2A1(j))))^2+(...
                        g+1)/(g-1);

                    u3as(i,j)= term1a(i,j)+sqrt(term2a(i,j));
                    asu3(i,j)= 1/u3as(i,j);
                    M3(i,j)=sqrt(2/((g+1)*(asu3(i,j))^2-g+1));
                        p3p1(i,j)=((1+(g-1)/2*M1(i)^2)^(g/(g-1)))/((1+(g...
                            -1)/2*(M3(i,j))^2)^(deff*g/(g-1)));
                    %%%%%%%% p4/p3 p3/p0 p4/p0
                        p4p3(i,j)=(1+(g-1)/2*M3(i,j)^2)^(deff*g/(g-1));
                        p3p0(i,j)=p3p1p(i,j)*p1p0(i);
                        p4p0(i,j)=p1p0(i)*p3p1p(i,j)*p4p3(i,j);
                    %calculation velocities
                            u1(i)=1/asu1(i)*astar;
                            u2(i)=1/(asu2(i))*astar;
                            u3(i,j)=u3as(i,j)*astar;

A1At(i,j)=A2A1(j)*1/A2At(i);
A1A3(i,j)=A1At(i,j)*AtA3(i,j);
```

```
A2A3(i,j)=1-A1A3(i,j);
p3(i,j)=p3p1p(i,j)*p1(i);
                end
end
```

B.2 nozzle_flow_isentropic.m

```
clear all

x0 = 0;
x1 = 1;
y0 = 0;
y1 = 1;
xx =linspace(0,1);
yy = spline([x0,x1],[y0,y1],xx);
yy = spline([x0,x1],[0,y0,y1,0],xx);

%y and x values of start, throat and end point. Change a2 for different
%exit area ratio
a0 = 2;
at = 0.25;
a2 = 0.4;
x0 = 0;
xt = 4;
x2 = 12;
g=1.4;
%define x range and add linear spacing
xx_0t = linspace(x0,xt);
xx_t2 = linspace(xt,x2);
%define spline from point 0 to throat and throat to end point with
%horizontal begin and connection point
yy_0t = spline([x0,xt],[0,a0,at,0],xx_0t);
yy_t2 = spline([xt,x2],[0,at,a2,0],xx_t2);
%plot nozzle
figure(1)
hold on;
plot(xx_0t,yy_0t);
xlabel('x')
ylabel('y')
plot(xx_t2,yy_t2);
plot(xx_t2,-yy_t2);
plot(xx_0t,-yy_0t);
hold off

%Area and pressure as a function of Mach number
a_as = @(M) 1./M.*(2/(g+1)*(1+(g-1)/2.*M.^2)).^((g+1)/(2*(g-1)));
p_p0 = @(M) (1+(g-1)/2*M.^2).^(-g/(g-1));
%Define M range for sub- and supersonic
M_super = linspace(1,4,3000000);
M_sub = linspace(0.00,1,1000000);
```

```
a0_at = a0/at;
a_at_0t = yy_0t/at;
a_at_t2 = yy_t2/at;

%Define M range for sub- and supersonic
M_super = linspace(1,4,10000);
M_sub = linspace(0.00,1,10000);

%Shift down the graph/vec with a0/at so right minimum where it croses 0 ...
    can
%be found
a_as_super = a_as(M_super);
a_as_sub = a_as(M_sub);
a_vec_sub = a_as_sub - a0_at;
a_vec_super = a_as_super - a0_at;


%loop for calculating every A/A* with the corresponding M
for i=1:numel(a_at_0t);
    a_vec2_sub = (a_as_sub - a_at_0t(i)).^2;
    [val_sub,loc_sub]=min(a_vec2_sub);
    M_conv(i)=M_sub(loc_sub);
end;
for j=1:numel(a_at_t2);
    a_vec2_super = (a_as_super - a_at_t2(j)).^2;
    [val_super,loc_super]=min(a_vec2_super);
    M_diver(j)=M_super(loc_super);
end;

%substitut M in Pressure formula
p_p0_sub = p_p0(M_conv);
p_p0_super = p_p0(M_diver);


%Plot M vs x
figure(2)
hold on
plot(xx_0t,M_conv)
plot(xx_t2,M_diver)
xlabel('x')
ylabel('M')
hold off
%plot pressure ratio vs x
figure(3)
hold on
plot(xx_0t,p_p0_sub)
xlabel('x')
ylabel('p/p0')
plot(xx_t2,p_p0_super)
hold off
```

B.3 massflow_throat.m

```
% close all
% clear all
% clc

pspi=0.01:0.0001:1;%ps/pi
2068427.19*0.5283
Ts=298
V=1557.43 %m^3
g=1.4;
A1=0.22
Ata=0.011/3.937161941987262
R=287
pip0=2068427.19/101325
for m=1:length(pspi)%fixed at t vs pspi
ta(m)=(-2*V*((pspi(m))^((1-g)/(2*g))-1))/((1-g)*R*sqrt(Ts)*Ata*sqrt(g/R...
    *(2/(g+1))^((g+1)/(g-1))));%isentropic
end

figure(1)
hold on
plot(ta,pspi*2068427.19,'g')
title('Pressure drop in Compressor storage tank')
xlabel('t(s)')
ylabel('ps(Pa)')


M1=0.85:0.05:0.85;
t=0:1:12000;
for i=1:length(M1)
for n=1:length(t)%fixed At pspi vs t
pspia(n)=(t(n)*((1-g)*R*sqrt(Ts)*Ata*sqrt(g/R*(2/(g+1))^((g+1)/(g-1))))...
    /(-2*V)+1)^(2*g/(1-g));
la(n)=pspia(n)*pip0;
M2(i,n)=sqrt((la(n)^((g-1)/g)*2*(1+(g-1)/2*M1(i)^2)-2)/(g-1));
A2At(i,n)=sqrt(1/M2(i,n)^2*((2/(g+1))*(1+(g-1)/2*M2(i,n)^2))^((g+1)/(g-1))...
    );
A2(i,n)=A2At(i,n)*Ata;
p2ps(i,n)=(1+(g-1)/2*M2(i,n)^2)^((-g)/(g-1));
A2A1(i,n)=A2At(i,n)*Ata/A1;
% p2(i,n)=p2ps(i,n).*pspia(n)*2068427.19;
%A2At(i,n)=sqrt(1/M2(i,n)^2*((2/(g+1))*(1+(g-1)/2*M2(i,n)^2))^((g+1)/(g-1)...
    ));%Fixed
%At in pspia
a(n)=1/t(n)*t(n);
end
end
```

Bibliography

[1] International Air Transport Association (December 2013). *Air passenger market analysis.* [Online]. Retrieved from www.iata.org/publications/economics/Documents/passenger-analysis-dec2013.pdf

[2] International Air Transport Association (December 2013), *Airlines Expect* 31% *Rise in Passenger Demand by 2017.* [Online]. Retrieved from www.iata.org/pressroom/pr/pages/2013-12-10-01.aspx

[3] Hu N., Buchholz H., Herr M., Spehr C., and Haxter, S. (2013). Contributions of Different Aeroacoustic Sources to Aircraft Cabin Noise, *19th AIAA/CEAS Aeroacoustics Conference.*

[4] Dr. J. Syms, Private correspondence, July-October 2014

[5] Kane R.F. and Kelley E.F. (1943). *The Theory, Design and Performance of a Two Dimensional High Speed, Induction Type, Wind Tunnel* (Unpublished master's thesis), California Institute of Technology, Pasadena, California, USA.

[6] Watanawanavet S. (2008). *CFD optimization study of high-efficiency jet ejectors* (Ph.D. thesis), Texas A&M University, College Station, Texas, USA.

[7] Bhat, W.V. (1971). Flight test measurement of exterior turbulent boundary layer pressure fluctuations on Boeing model 737 airplane. *Journal of Sound and Vibration*, 14(4), 439-457.

[8] Prof.dr.ir. H.W.M. Hoeijmakers, Gasdynamics Lecture notes - Part IV, University of Twente

[9] Bartosiewicz, Y., Aidoun, Z., Desevaux, P., and Mercadier, Y. (2005). Numerical and experimental investigations on supersonic ejectors. *International Journal of Heat and Fluid Flow*, 26(1), 56-70.

[10] Holtzapple, M. T. (2001). *High-Efficiency Jet Ejector* (Invention Disclosure), Department of Chemical Engineering, Texas A&M University, College Station, Texas, USA.

[11] Pope, A., Goin, K.L. (1978). *High-Speed Wind Tunnel Testing* (pp. 127). Huntington, New York, USA: R. E. Krieger Publishing Company.

[12] Kim, H.D. et al. (2013). Application of Chevron nozzle to a supersonic ejector/diffuser system. *Procedia Engineering*, 56, 193-200.

[13] Chang, Y.J., Chen, Y.M. (2000). Enhancement of a steam-jet refrigerator using a novel application of the petal nozzle. *Experimental Thermal and Fluid Science*, 22, 203-211.

[14] Eames, I.W. (2002). A new prescription for the design of supersonic jet-pumps: the constant rate of momentum change method. *Applied Thermal Engineering*, 22, 121-131.

[15] Palani, K. et al. (2013). Enhancement of Entrainment Ratio in Jet Pump using Constant Rate of Momentum Change Diffuser. *International Journal of Thermal Technologies*, 3(1).

[16] Kim, H.D. et al. (2012). Computational Analysis of Mixing Guide Vane Effects on Performance of the Supersonic Ejector-Diffuser System. *Open Journal of Fluid Dynamics*, 2, 45-55.

[17] Kim, H.D. et al. (2006). Optimization Study of a Coanda Ejector. *Journal of Thermal Science*, 15(4), 331336.

[18] Nex flow, Air amplifiers (September 2014). [Online]. Retrieved from http://www.nex-flow.com/pdf_nex_flow/air_amplifier.pdf